Complex dielectric constant of sea foam at microwave frequencies

Magdalena D. Anguelova[1]

Received 12 March 2007; revised 14 April 2008; accepted 18 April 2008; published 1 August 2008.

[1] We present a systematic investigation of the applicability of a group of mixing rules for obtaining the dielectric constant (permittivity) of sea foam (whitecaps) at microwave frequencies, 1.4 to 37 GHz. By demonstrating that the foam scattering is weak at these frequencies, we justify our interest in basic mixing rules, which do not involve explicit scattering computation, namely, the Maxwell Garnett, Polder-Van Santen, Coherent potential, Looyenga, and Refractive models. The complex dielectric constant of sea foam obtained with these mixing rules is presented and the dependence of foam permittivity on foam void fraction, radiation frequency, sea surface temperature, and salinity is reported. With the exception of the Coherent potential model, all selected mixing rules give reasonable values for the sea foam dielectric constant. To further examine the suitability of a permittivity model for computing the dielectric constant of sea foam, the performance of each mixing rule is evaluated on the basis of three criteria: (1) how well a permittivity model deals with a wide range of void fractions, (2) how a permittivity model behaves approaching the foam-air and foam-water boundaries, and (3) how the choice of a permittivity model affects estimates of emissivity and brightness temperature due to foam. The suitability of the basic mixing rules for computing the complex dielectric constant of sea foam at microwave frequencies can be ranked as: (1) Refractive model, (2) Looyenga model, (3) Maxwell Garnett model, and (4) Polder-Van Santen model.

Citation: Anguelova, M. D. (2008), Complex dielectric constant of sea foam at microwave frequencies, *J. Geophys. Res.*, *113*, C08001, doi:10.1029/2007JC004212.

1. Introduction

[2] Increasing demands for accuracy in geophysical retrievals from passive microwave measurements necessitate developing forward geophysical models capable of adequately accounting for the foam effects. To model the effects of foam, one needs a model for the foam emissivity and a parameterization for the foam fraction (whitecap coverage). Thus, with two scientific goals in mind, pursued within the framework of the WindSat mission at the Naval Research Laboratory [*Gaiser et al.*, 2004; *Bettenhausen et al.*, 2006], namely, estimate the foam fraction from microwave satellite measurements and include explicitly the effect of sea foam in a future WindSat forward model, we started work on modeling the foam emissivity, e_f, at frequencies from 6.8 GHz to 37 GHz. Since foam influences salinity measurements [*Font et al.*, 2003; *Camps et al.*, 2005], we also consider the frequency of 1.4 GHz.

[3] The quantities necessary for computing e_f are attenuation in the foam and transmission and reflection at foam-air and foam-seawater boundaries. To obtain those quantities, one needs the complex relative dielectric constant (permittivity) of the sea foam, $\varepsilon_f = \varepsilon_f' - j\varepsilon_f''$. (Hereinafter we omit the word "relative".) The imaginary part, $\mathrm{Im}\{\varepsilon_f\} = \varepsilon_f''$, is a measure of the attenuation due to absorption and scattering in foam. The absorption losses in foam arise from the presence of seawater with its high conductivity, while the individual bubbles comprising the foam induce scattering losses. Meanwhile, both the real, $\mathrm{Re}\{\varepsilon_f\} = \varepsilon_f'$, and the imaginary components are essential for determining the transmission and reflection at the foam boundaries. Since the seawater content in the foam controls the values of ε_f' and ε_f'', foam void fraction, f_a, defined as the fraction of a unit volume of seawater that is occupied by air, is the most important quantity characterizing the sea foam as a medium.

[4] As will be shown, specific features of the sea foam floating on the ocean surface are (1) a wide range of void fractions for each of the mixture constituents (air and seawater) and (2) absorption and scattering taking place within densely packed air bubbles. Thus, to be applicable to sea foam, a permittivity model aiming to predict ε_f needs to treat these specific features accordingly. To address these features, previous foam emissivity models compute the attenuation and the permittivity in foam with various scattering theories using as input the microscopic characteristics of foam such as bubble diameters, bubble wall thicknesses, bubble size distribution, filling factor, and stickiness parameter [*Raizer and Sharkov*, 1981; *Guo et al.*, 2001; *Chen et al.*, 2003; *Raizer*, 2007]. Uncertainties introduced via the many parameters required for the computation of scattering losses in foam affect the accuracy of

[1]Remote Sensing Division, Naval Research Laboratory, Washington, DC, USA.

foam emissivity models. Moreover, while mathematically rigorous, scattering models are computationally expensive for use in operational retrieval algorithms or for processing large data sets.

[5] To restrict uncertainty and facilitate use in retrieval algorithms, it is more practical to develop a foam emissivity model using exclusively macroscopic quantities characterizing the sea foam, namely void fraction profile and foam-layer thickness. Circumventing the use of microscopic quantities, we forego explicit modeling of the scattering losses in foam. Thus we can obtain ε_f employing one of the classical permittivity models (aka mixing rules), which involve only the seawater permittivity, ε, air permittivity, $\varepsilon_0 = 1 - j0$, and f_a. To pursue such a modeling strategy, however, we need to consider: (1) if attenuation due to scattering in foam can be ignored and (2) what limitations such a simplification may pose on the applicability of known classical permittivity models in the range of the considered frequencies. Until now the only classical permittivity model applied to sea foam is the well-known Maxwell Garnett formula. Moreover, in some instances it has been used only with high void fractions [*Droppleman*, 1970; *Rosenkranz and Staelin*, 1972; *Wentz*, 1974]. None of the previous studies, however, justifies the use of this formula in the range beyond its supposed applicability (i.e., low f_a), or assesses its advantages over other mixing rules, or analyzes the sensitivity of the emissivity models to the choice of a particular permittivity model.

[6] The aim of the present study is to address the questions formulated above and identify mixing rule(s) potentially suitable for computing the dielectric constant of sea foam, ε_f, thus the corresponding foam emissivity, e_f. In the process we attempt to further the understanding of sea foam as a dielectric medium and provide a reference for the main dependencies of the sea foam on void fraction, radiation frequency, sea surface temperature (SST), and salinity.

[7] Ideally, conclusions regarding the most suitable model for the dielectric constant of sea foam should be based on comparisons with dielectric measurements. It is difficult to conduct dielectric measurements since suitable methods need to be identified and specific apparatus to be built for each frequency [*Ellison et al.*, 1996]. For the case of sea foam, creating and controlling specific samples would add to those difficulties. Thus no direct observations of sea foam permittivity have been conducted and reported. Our approach, therefore, relies on previous findings on various heterogeneous dielectric mixtures and reported characterizations of sea foam in order to evaluate as well as possible the applicability of various permittivity models for obtaining acceptable predictions of the sea foam dielectric constant.

[8] Previous results and conclusions drawn from them for the sea foam are given in sections 2 and 3. Section 2.1 defines sea foam as an oceanographic and microwave-remote-sensing subject. A review of oceanographic measurements describes the mechanical structure and characteristics of sea foam (section 2.2), which determine foam dielectric properties. A survey of reported results from microwave measurements and models (section 2.3) establishes the dominance of the absorption over scattering in foam, which justifies ignoring scattering attenuation and using classical mixing formulae for the foam permittivity. In sections 3.1–3.4, we summarize current knowledge of the effective medium theory with respect to classical mixing rules and use the findings to identify a pattern of behavior for heterogeneous mixtures from which we infer an expected behavior for sea foam. Section 3.5 justifies the selection of five mixing rules to be investigated in this study. The original contribution consists of applying and analyzing the selected mixing rules in the context of sea foam (section 4) and judging their suitability for obtaining the foam permittivity using three criteria (section 5).

2. Sea Foam as a Dielectric Medium

2.1. Sea Foam

[9] Sea foam, manifested in the ocean as whitecaps, forms when ocean waves break and force air into the water. The entrained air ruptures into a cloud of bubbles with a wide range of sizes [*Blanchard and Woodcock*, 1957; *Kolovayev*, 1976; *Koga*, 1982; *Baldy*, 1988; *Wu*, 1994; *Deane and Stokes*, 2002]. The smallest bubbles quickly dissolve and disappear, while larger and more buoyant bubbles rise to the surface forming, and constantly replenishing, floating bubble rafts. Both the bubble clouds (also called bubble plumes) below the surface and the froth on the surface are considered sea foam [*Adamson*, 1997, p. 519].

[10] The surface part of the whitecaps bears further distinction. At the moment of active breaking, the whitecaps are thick and bright (visually and radiometrically), sit at and travel with the wave crest, and cover less area. This actively generated sea foam is referred to as stage A (young) whitecaps [*Monahan and Woolf*, 1989]. In contrast, the foam decaying after the breaking event and the froth formed by the bubbles rising from below are thinner and less bright, linger behind the wave that has created them, and spread over a larger area. This residual sea foam is referred to as stage B (mature) whitecaps. *Lewis and Schwartz* [2004, p. 259] give an account of the various terms used in the literature for active and residual foams. The wind-generated foam in both randomly scattered whitecap patches (especially those of longer-lived residual foam) and the submerged bubble plumes associated with those patches have been observed to organize into streaks (or rows) under moderate, but persistent wind due to Langmuir circulation [*Thorpe*, 1984; *Pinet*, 1992].

[11] For any passive remote sensor the bulk of the registered radiation emanates from the upper part of the water column or the skin depth, defined as the medium thickness over which the electromagnetic radiation decreases by a factor of $1/e$ [e.g., *Ulaby et al.*, 1986, p. 1420]. For the considered microwave frequencies, the skin depths of foam-free seawater are from around 0.5 mm up to 10 mm. Note that this electromagnetically defined skin depth is an entity different from the cool skin of the ocean surface (a few millimeters) caused by net upward heat flux due to molecular conduction [*Fairall et al.*, 1996; *Jessup et al.*, 1997]. Also, being frequency dependent, the skin depth at microwave frequencies is thicker compared to the skin depth (termed also optical depth) at infrared frequencies (a few microns to at most a millimeter) used for SST measurements and infrared remote sensing of breaking waves [*Jessup et al.*, 1997].

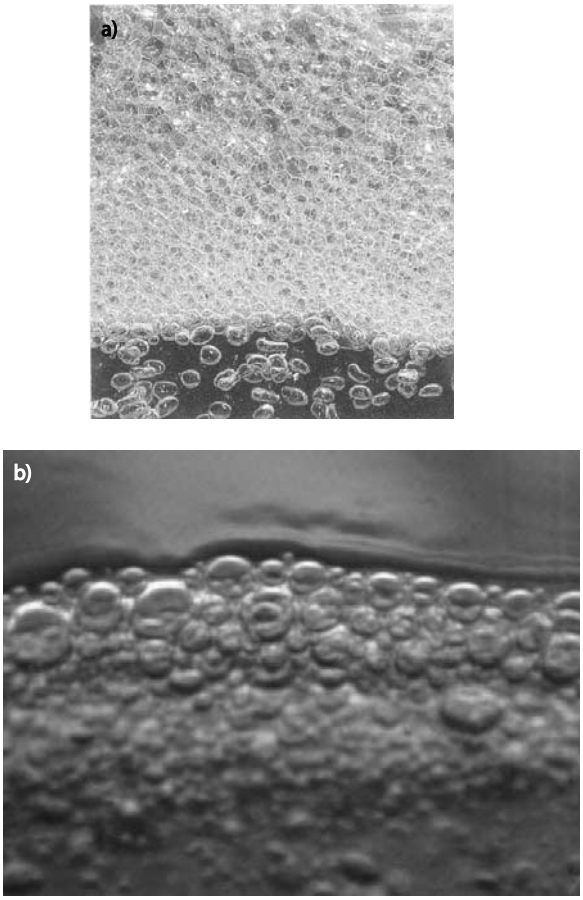

Figure 1. Surface foam layer and the bubbles within for (a) simulated foam formed by sparing air through porous plate and stabilized with surfactants (photo courtesy of Prof. Jan J. Cilliers, chair in Mineral Processing, Department of Earth Science and Engineering, Imperial College London, London, UK) and (b) natural foam formed by wave breaking in seawater (photo courtesy of William E. Asher, senior oceanographer at Applied Physics Laboratory, University of Washington, Seattle, WA).

[12] The microwave skin depth increases as air is mixed with the seawater to form foam. Estimates show that for a foam-covered surface, depending on the air content of the foam, the skin depth may range from less than 1 mm at 37 GHz to more than a few meters (if such foam layers exist) at lower frequencies. Reviewing field measurements for bubble plume depths [e.g., *Thorpe*, 1982; *Walsh and Mulhearn*, 1987; *Wu*, 1994; *Melville et al.*, 1995; *Dahl and Jessup*, 1995] and laboratory measurements for foam layer thicknesses [*Militskii et al.*, 1977; *Peltzer and Griffin*, 1988; *Reising et al.*, 2002; *Camps et al.*, 2005], we expect that in open ocean, depending on the wind speed, the foam thickness at the surface, not the bubble plumes, may range from 1 cm to more than 12 cm in newly-formed whitecaps and from 0.1 to 1 cm when the whitecaps decay. Therefore, at frequencies from 10 to 37 GHz, the subject of interest in remote sensing studies narrows to the foam layers on the surface, excluding the deeper bubble plumes. The lower frequencies (1.4 and 6.8 GHz) have the potential to ''feel'' deeper bubble plumes. This study focuses on the foam layers floating on the surface, thin or thick, and the dense bubbly mixture immediately below (Figure 1).

2.2. Void Fraction of Sea Foam

[13] At any instant there is a distribution of foam thicknesses in the open ocean resulting from wave breaking under different meteorological and environmental conditions and temporal evolution of the sea foam from young to mature [*Reul and Chapron*, 2003]. While foam thickness, t, affects strongly e_f and is a necessary quantity for obtaining it, t is not directly involved in obtaining the foam permittivity ε_f. Thus the study presented here focuses on the $\varepsilon_f(f_a)$ relation and its effect of e_f, while the relation $e_f(t)$ at a chosen $\varepsilon_f(f_a)$ will be investigated in detail elsewhere. However, examining how f_a changes with t helps to identify the range of f_a values, which, in turn, determine ε_f.

[14] At any stage of whitecap lifetime, from formation to decay, foam void fraction changes significantly with depth, from $f_a \approx 100\%$ at the interface adjacent to the air to $\ll 1\%$ at the interface adjacent to the seawater and below. The reason is that the foam structure changes in depth. Figure 1 illustrates this change in depth for soap foam (a) and natural foam (b). As the images in Figure 1 show, the upper part of a foam layer has high void fraction because it is composed of densely packed, large, differently shaped bubbles divided with thin liquid films (dry foam). Below the air-foam interface, the void fraction gradually decreases with increasing depth as the foam composes smaller and more spherical bubbles with thicker walls, a structure containing more water (wet foam). Still further down below the surface foam layer, the bubble walls swell with so much water that the bubbles separate completely forming a plume. Though for different reasons, buoyancy or coarsening, both young and aged foams exhibit such a structure.

[15] *Droppleman* [1970] considers high void fraction value in sea foam, say above 90%, ''intuitively a feasible value''. Thus previous foam emissivity models have used values around 99% [e.g., *Rosenkranz and Staelin*, 1972; *Wentz*, 1974]. Laboratory measurements of simulated foam report void fraction values over the full range, from 0 to 1 [*Bordonskiy et al.*, 1978; *Camps et al.*, 2005]. *Rose et al.* [2002] experimentally measured void fraction of 85% in the center of an artificially generated foam layer and, following *Droppleman*'s [1970] suggestion, expected a value of 95% at the top of the layer. However, the highest void fraction value reported for breaking waves is 40% in laboratory [*Lamarre and Melville*, 1991] and 65% in field [*Gemmrich and Farmer*, 1999] experiments. Higher void fraction values in open ocean conditions have not been observed. Moreover, Figure 1b implies that the dry-foam stage may not be attainable in breaking waves since the bubbles are more rounded and thick-walled compared to bubbles in simulated foam (Figure 1a). It is, however, plausible that high void fraction values from field experiments are missing not because a dry-foam stage does not exist, but because it is short lived and because it is difficult to probe well a foam layer floating on a wavy surface. Thus, to ensure that foam permittivity values and the corresponding emissivity model will be applicable to cases of active and residual foam, we work with the full range of void fractions: f_a from 0 to 1.

[16] We conclude that, because of its mechanical structure, the sea foam floating on the ocean surface is charac-

terized by a wide range of void fractions and densely packed air bubbles. These are the salient physical properties defining foam as a dielectric medium and need to be addressed in the foam permittivity, ε_f, and the corresponding foam emissivity, e_f, models. Modeling the effects of both these features on the absorption and scattering in foam is a formidable task requiring a number of microscopic characteristics describing the bubble population that composes the sea foam.

[17] Numerous laboratory and field observations have characterized deep bubble plumes well [e.g., *Kolovayev*, 1976; *Thorpe*, 1982; *Baldy*, 1988; *Wu*, 1994; *Dahl and Jessup*, 1995; *Leifer and de Leeuw*, 2006; *Leifer et al.*, 2006]. In contrast, measurements characterizing the surface foam layers are few and usually of simulated, not natural, sea foam [*Militskii et al.*, 1978; *Peltzer and Griffin*, 1988; *Rose et al.*, 2002; *Camps et al.*, 2005]. Not knowing confidently the microscopic foam characteristics from experiments, we attempt to model ε_f and e_f using exclusively macroscopic foam characteristics, such as void fraction and foam thickness, by ignoring scattering losses in foam. The simplification of ignoring the scattering is next justified by a review of experimental and modeled radiometric data.

2.3. Absorption and Scattering in Sea Foam

[18] Seawater is a lossy medium because of its high conductivity. Its presence in foam prescribes high absorption losses, thus high thermal emission from foam-covered areas. Meanwhile, bubbles forming the foam lead to scattering losses. Though scarce, previously published experimental and modeled results clearly reveal that of these two processes, absorption (thus emission), not scattering, is the process that defines the overall signal emanating from foam-covered surfaces at most of the frequencies of current space-based radiometers.

2.3.1. Experimental Observations

[19] *Williams* [1971] employs an active technique at a wavelength of 3.2 cm (9.4 GHz) to measure the microwave emissivity of artificial foam layers spread over different substrates. The emissivity of foam layers floating on a water surface increases from 0.6 to 0.95 as the foam thickness changes from a monolayer of bubbles to a few millimeters. By contrast, the change of emissivity from foam with the same thicknesses spread on an aluminum plate is "surprisingly low". *Williams* [1971] concludes that "scattering is not a major factor in the effects we measured." Moreover, the results due to the difference in the substrates underlying the foam, water or metal, suggest that not just the foam itself, but the combination of foam floating on water is the system that provides high emissivity.

[20] *Militskii et al.* [1978] measure at a wavelength of 0.8 cm (37.5 GHz) the time evolution of thermal radio emission from artificial foam left to decay naturally from a thickness of more than 1 cm to a thin monolayer of bubbles ($\leq$0.1 cm). Their results show that about 85–90% of the increase of brightness temperature was due to just the thin monolayer of bubbles. The dry foam above the monolayer contributes no more than 15% to the radio emission despite its greater thickness. *Militskii et al.*'s [1978] observation suggests that: (1) the attenuation in dry foam due to absorption and scattering is not significant and (2) the thin, wet foam layer close to the foam-water boundary plays a defining role for the signal from foam-covered areas.

[21] Using the same experimental setup as that described by *Militskii et al.* [1978], *Bordonskiy et al.* [1978] report results for the emissivity of soap foam (as in Figure 1a) at multiple wavelengths (frequencies): 0.26, 0.86, 2.08, 8, and 18 cm (115.3, 34.9, 14.4, 3.7, 1.7 GHz, respectively). Though revealing frequency dependence, the experimental data generally confirm the observation reported by *Militskii et al.* [1978]: the thin layer causes the major change in the emissivity coefficient over that of smooth water. This observation is consistent for all frequencies, low and high, when we consider the ratios of the thin and thick layers, used in the experiment, to the wavelengths.

2.3.2. Modeling Results

[22] *Dombrovskiy* [1979, 1982] calculates using Mie theory the absorption, scattering and extinction efficiency factors (Q_a, Q_s, and Q_e, respectively) for spherical water bubbles with different sizes and wall thicknesses. The results show that the values of Q_a and Q_e are very close at λ = 8.6 mm (34.9 GHz) and "practically coincide at $\lambda \geq$ 20.8 mm" ($\leq$14.4 GHz). This implies that absorption in bubble walls is the main attenuating factor and further clarifies conclusion (1) from *Militskii et al.*'s work that the observed small attenuation in dry foam is predominantly due to absorption within the bubble walls, not scattering. Scattering, however, increases as radiation frequency and bubble dimensions (radius and wall thickness) increase.

[23] *Chen et al.* [2003, their Tables II–IV] calculate absorption, scattering, and extinction coefficients (k_{abs}, k_s, and $k_e = k_{abs} + k_s$, respectively) on the basis of Monte Carlo simulations of dense media. At 10.8 GHz, absorption in foam contributes 95% to 99% to k_e. At 36.5 GHz, k_s in foam adds up to 13% to the total extinction for small bubbles (radii $\leq$0.5 mm). The most significant scattering losses are at 36.5 GHz for foam comprising the largest bubbles under consideration (1 mm radius), which is consistent with the results of *Dombrovskiy* [1979, 1982].

[24] *Zhang et al.* [2003] calculated extinction and scattering, hence absorption, coefficients (k_e, k_s, $k_a = k_e - k_s$, respectively) at 19.35 GHz for foam consisting of large bubbles (inner radius of 4.3 mm) with relatively thick walls (0.13 mm). In the model, the foam layer is assumed to be much thicker than the penetration depth of the radiation, thus excluding the emissivity of the water below the foam layer. Therefore, considering the processes in the foam layer alone [*Zhang et al.*, 2003, equation (30)], these results represent a numerical analog of the experiment by *Williams* [1971] for foam spread over an aluminum plate. Eliminating a major contributor to absorption (the water below the foam) and considering large thick-walled bubbles at relatively high frequency, the model, not surprisingly, predicts low absorption (about 28% of the total extinction) and significant scattering, which is consistent with the other analytical and experimental findings.

[25] The point of this detailed review is to demonstrate that at the considered frequencies (1.4 to 37 GHz) scattering in natural sea foam is weak with a single scattering albedo less than 0.1. The absorption determines the attenuation in the foam-water system and in the foam layer itself. Ignoring scattering, the signal due to a foam-covered surface will be underestimated by no more than 15% at higher frequencies

Table 1. Mixing Rule formulae [*Sihvola*, 1999; *Ulaby et al.*, 1986, Appendix E] for the Effective Permittivity ε_{eff} of a Mixture With Environment and Inclusions Permittivities ε_e and ε_i, Respectively, and Inclusion Volume Fraction f_v

Unified Formula	In Foam Notations[a]
$\dfrac{\varepsilon_{eff}-\varepsilon_e}{\varepsilon_{eff}+2\varepsilon_e+\nu(\varepsilon_{eff}-\varepsilon_e)}=f_v\dfrac{\varepsilon_i-\varepsilon_e}{\varepsilon_i+2\varepsilon_e+\nu(\varepsilon_{eff}-\varepsilon_e)}$	
$\nu = 0$ Maxwell Garnett (MG)	$\varepsilon_f=\varepsilon\left[1-\dfrac{3f_a(\varepsilon-1)}{1+2\varepsilon+f_a(\varepsilon-1)}\right]$
$\varepsilon_{eff}=\varepsilon_e+3f_v\varepsilon_e\dfrac{\varepsilon_i-\varepsilon_e}{\varepsilon_i+2\varepsilon_e-f_v(\varepsilon_i-\varepsilon_e)}$	Using $Q = 1 - f_a$ obtain the form of *Rosenkranz and Staelin* [1972] and *Wentz* [1974]
	Using $y = (1-\varepsilon)/(1+2\varepsilon)$ and $\varepsilon_0 = 1$ the form of *Guo et al.* [2001] $2\varepsilon_f^2+\varepsilon_f[1-2\varepsilon+3f_a(\varepsilon-1)]-\varepsilon=0$
$\nu = 2$ Polder-van Santen (PS)[b]	
Bruggeman or de Loor formula	$3\varepsilon_f^2+\varepsilon_f[1-4\varepsilon+4f_a(\varepsilon-1)]-\varepsilon(1-\varepsilon)(1-f_a)=0$
$\nu = 3$ Coherent Potential (CP)[b]	
Power law formulae: $\varepsilon_{eff}^{\beta}=f_v\varepsilon_i^{\beta}+(1-f_v)\varepsilon_e^{\beta}$	
$\beta \to 0$ Logarithmic law	$\varepsilon_f=\varepsilon^{1-f_a}$
$\ln\varepsilon_{eff}=f_v\ln\varepsilon_i+(1-f_v)\ln\varepsilon_e$	
Lichtenecker formula	
$\beta = 1$ Linear law	$\varepsilon_f=f_a+(1-f_a)\varepsilon$
Average dielectric constant model or Silberstein formula	
$\beta = 1/2$ Quadratic law Refractive model or	$\sqrt{\varepsilon_f}=f_a+(1-f_a)\sqrt{\varepsilon}$
Beer formula or Birchak formula	$=\left[f_a+(1-f_a)\varepsilon^{\frac{1}{3}}\right]^3$
$\beta = 1/3$ Cubic law Looyenga formula	

[a]In foam notations, use $\varepsilon_{eff}\equiv\varepsilon_f$, $\varepsilon_e\equiv\varepsilon$, $\varepsilon_i\equiv 1$, and $f_v\equiv f_a$.
[b]The choice in the solutions of the PS and CP equations is resolved by noting that the Re and Im parts of ε_f must be positive.

(e.g., 37 GHz), and often much less, if at all, at lower frequencies. This suggests that the classical mixing rules, which do not account for the scattering losses explicitly, could be applied to foam. Hereinafter we use the expression "classical mixing rules" to indicate lack of explicit scattering modeling.

3. Classical Mixing Rules

3.1. Effective Medium Theory

[26] Being a medium composed of air and seawater, the sea foam is a heterogeneous mixture whose dielectric behavior can be predicted with a suitable mixing rule. Enlisting different approaches to derive various mixing rules, the effective medium theory (EMT) is a useful tool for predicting and analyzing the dielectric and radiative properties of composite materials [*Choy*, 1999]. The mixing rules relate the effective permittivity ε_{eff} of a heterogeneous mixture to the permittivities of its components [*van Beek*, 1967; *Ulaby et al.*, 1986, Appendix E; *Sihvola*, 1999]. In two-phase mixtures like sea foam, the components are described as an environment with inclusions, each with permittivity ε_e and ε_i, respectively. The volume fraction f_v of the total mixture volume occupied by the inclusions controls the nature and character of the mixture. For sea foam, we assign seawater as the environment and air bubbles as inclusions thus denoting $\varepsilon_{eff}\equiv\varepsilon_f$, $\varepsilon_e\equiv\varepsilon$, $\varepsilon_i\equiv 1$, and $f_v\equiv f_a$. Most natural media are material-in-air mixtures with a dielectric contrast $\varepsilon_i/\varepsilon_e > 1$ ($\varepsilon_e\equiv\varepsilon_0 = 1 - j0$) and have been more extensively studied than air-in-material mixtures, like the sea foam, with $\varepsilon_i/\varepsilon_e < 1$.

[27] EMT has promoted numerous mixing rules [*Sihvola*, 1999] (Table 1). Widely used is the well-known Maxwell Garnett (MG) formula. The Polder-Van Santen (PS) and the Coherent potential (CP) formulae are for dense media in which dipole interactions and multiple scattering between closely packed inclusions need to be accounted. A wide class of mixing formulae uses power law presentation, namely Beer mixing rule (aka Birchak formula or refractive or quadratic model), Looyenga formula (or cubic model), the linear model (aka Silberstein formula or average dielectric constant), and the Lichtenecker model (logarithmic law). The question is which of the many available mixing rules has the potential to predict the foam permittivity consistently.

[28] The MG formula is the only classical mixing rule used in previous foam studies [*Droppleman*, 1970; *Rosenkranz and Staelin*, 1972; *Wentz*, 1974; *Guo et al.*, 2001, region 2 in their Figure 3; *Camps et al.*, 2005, for region 2 in their Figure 1]. The apparent impression that different mixing formulae have been applied to obtain sea foam permittivity is removed when with appropriate notations of the variables and some algebraic re-arrangement it is shown that many formulae published in the literature reduce to the expression for MG rule, namely: (1) Rayleigh mixing formula [*Sihvola and Kong*, 1988, equation (6)]; (2) formula derived by *Odelevskiy* [1951, equations (8) and (19)] for various properties (density, permittivity, conductivity) of a two-phase system whose inclusions have various shapes and volume fractions from 0 to 1; and (3) formula used by *Troitsky* [1962, equation (15)] for porous material. A modified form of the classical Lorentz-Lorentz formula [*Sihvola*, 1999, p. 47] has also been used in foam studies [*Raizer and Sharkov*, 1981; *Camps et al.*, 2005, region 1 in their Figure 1; *Raizer*, 2007]. However, abiding with our restriction to "classical models" in the sense of ignoring scattering, we do not consider it further.

3.2. Permittivity Bounds

[29] Predictions of the permittivity of various heterogeneous mixtures obtained with the formulae proposed by the EMT agree with experimental observations to a varying degree [*De Loor*, 1965]. *De Loor* [1983] thus concludes that it is impossible to choose one particular relation to fully

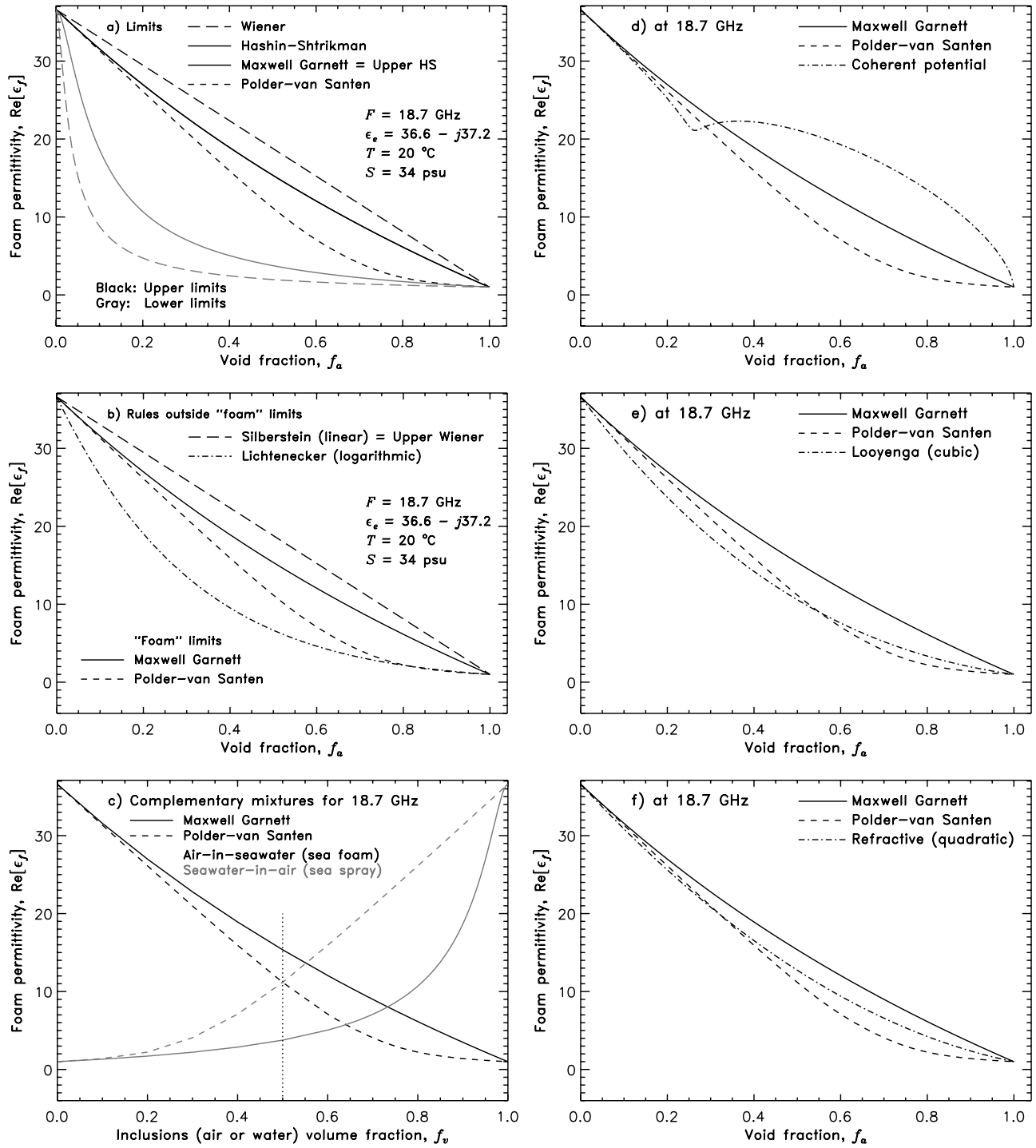

Figure 2. Foam permittivity (real part) as a function of foam void fraction for heterogeneous mixtures with $\varepsilon_i/\varepsilon_e < 1$ at 18.7 GHz. (a) Permittivity limits: Wiener (black and gray long-dashed lines) and Hashin-Shtrikman (black and gray solid lines). The upper Hashin-Shtrikman limit coincides with the Maxwell Garnett model. The lower Hashin-Shtrikman limit is improved by the Polder-Van Santen (short dashed line). (b) Mixing rules outside the limits for foam-like mixtures. The Maxwell Garnett (solid line) and the Polder-Van Santen (short-dashed line) models constitute the upper and lower limits for the sea foam. The Silberstein (linear) model is above the upper limit (long-dashed line); it coincides with the upper Wiener limit. The Lichtenecker (logarithmic) model is below the lower limit (dash-dot line). (c) Permittivity models (Maxwell Garnett and Polder-Van Santen) for complementary mixtures at 18.7 GHz: air-in-seawater (black lines) and seawater-in-air (gray lines) mixtures exemplifying sea foam and sea spray, respectively. (d) Coherent potential model (dash-dot line) compared to the foam limits. (e) Looyenga (cubic) model compared to the foam limits. (f) Refractive (quadratic) model compared to the foam limits.

describe the permittivity of a specific mixture. Such a choice is even more problematic when experimental data are not available for the mixture under investigation (as is the case for the sea foam). EMT alleviates this problem by establishing upper and lower bounds between which one can seek the true permittivity values of a mixture [*Kärkkäinen et al.*, 2000]. These bounds are expected to "come closer together the more is known about a particular mixture" [*De Loor*, 1983, p. 364].

[30] The most general bounds (Wiener bounds) are derived for mixtures with maximized and minimized permittivity (or conductivity) [*Sihvola*, 1999, p. 152] and enclose the largest area with allowed values for ε_{eff}. Figure 2a (black and gray long-dashed lines) illustrates the Wiener bounds for the real component of foam permittivity at 18.7 GHz. Formulated for the extreme dielectric properties of a mixture, the Wiener bounds are representative for an anisotropic mixture. Considering an isotropic mixture, *Hashin and Shtrikman* [1962] derive another set of upper and lower bounds employing variational theorems (see also *Choy* [1999, Chapter 2]). These new limits (aka Hashin-Shtrikman (HS) bounds) are not only stricter than the Wiener bounds, but prove to be the most restrictive ones that can be given in terms of ε_e, ε_i, and f_v. That is, any modeled or measured values for ε_{eff} of a given mixture most likely lie on or between the HS limits for this mixture. The solid black and gray lines in Figure 2a illustrate the HS limits for sea foam at 18.7 GHz.

[31] Recently *Kärkkäinen et al.* [2000] tested these two sets of limits by simulating thousands of samples for two different mixtures with the Finite-difference time-domain (FDTD) method, a popular computational technique used for electrodynamics modeling. As expected, the results show that all possible permittivity values are between the Wiener limits and almost always fall between the HS limits.

3.3. The Bounds for Foam-Like Mixtures

[32] For air-in-material mixtures with $\varepsilon_i/\varepsilon_e < 1$, the upper HS limit is equal to the MG mixing rule (black solid line in Figure 2a) for spherical inclusions [*Hashin and Shtrikman*, 1962; *Datta et al.*, 1993]. Using available measurements, *De Loor* [1965, 1983] finds that the lower HS limit (gray solid line in Figure 2a) is further improved by the PS mixing rule (short-dashed line in Figure 2a), constraining even more the range of possible ε_{eff} values for air-in-material mixtures. With the current EMT knowledge, therefore, we surmise that for sea foam the range of possible values for ε_f is the area enclosed between the MG and the PS mixing rules (solid and short-dashed black lines in Figure 2a, respectively).

[33] The PS mixing rule has two special traits as compared to the MG rule: (1) a symmetric treatment of the inclusions and the environment [*Sihvola*, 1999, p. 162] and (2) a well-defined percolation threshold. A consequence of the former is that the predictions of the dielectric constant of the mixture do not depend on the choice of each of the mixture components as an inclusion or as an environment. This is appealing when we recognize the fact that close to the sea foam boundaries the roles of seawater and air as environment or as inclusions interchange completely and the inclusion/environment choice is not unique. That is, we could consider dry (wet) foam as a large (small) amount of air imbedded in seawater or as a small (large) amount of seawater imbedded in air. However, no matter what our choice is for the inclusions and the environment (seawater-in-air or air-in-seawater), we would like to predict the same value for the dielectric constant of a foamy mixture with a fixed air-seawater content. This symmetry trait of the PS rule does not change when the inherent asymmetry of the foam void fraction in depth is accounted for (section 2.2 and Figure 1). This is verified and illustrated in Figure 2c by taking the inclusion volume fraction f_v to follow an exponential profile. Even with the asymmetric f_v profile, the curves for the air-in-seawater and seawater-in-air mixtures intersect at a point corresponding to 50% inclusion fractions, as should be for a symmetric formula [*Sihvola*, 1999, p. 162].

[34] The second trait of the PS formula is that it predicts a percolation threshold for heterogeneous mixtures. The percolation threshold, an important parameter for any mixture, represents the volume fraction around which the effective permittivity (or any other characteristics) of the mixture changes significantly [*Kirkpatrick*, 1973; *Hsu et al.*, 1988; *Sihvola et al.*, 1994; *Choy*, 1999, p. 13; *Sihvola*, 1999, p. 226]. In the instance of conductance, up to the critical value $f_v \cong f_c$ of the inclusions fraction, a mixture of insulating and conducting components (analogous to the air and seawater in sea foam) behaves as an insulator for small conductor inclusions ($f_v < f_c$); for inclusions fraction above the threshold value ($f_v > f_c$) the mixture abruptly changes its behavior to that of a conductor. For the PS rule, analytical reasoning leads to threshold value of $f_c \approx 1/3$ [*Sihvola et al.*, 1994, equation (8)]. In Figure 2c, this is exemplified for the permittivity of the sea spray (gray dashed line), whose slope changes noticeably around $f_c \approx 1/3$. Conversely, the mixture is more like a conductor for small insulator inclusions until the insulating component reaches a critical value (this time $1 - f_c \approx 2/3$) whence the mixture reverts to behave as an insulator. Figure 2c (black dashed line) demonstrates this case for the permittivity of the sea foam. Meanwhile the MG mixing rule does not clearly predict a threshold. The MG rule pushes the percolation threshold to $f_c = 1$ [*Sihvola*, 1999; *Sihvola et al.*, 1994], i.e., a conductive (insulating) mixture remains a conductor (insulator) until the insulating (conducting) inclusions completely replace the conductive (insulating) environment.

[35] It has been noted [*Choy*, 1999] and numerically confirmed [*Sihvola et al.*, 1994] that the theoretically determined percolation thresholds for various mixing rules are more clearly recognizable as the dielectric contrast of the mixture constituents increases. In addition, *Sihvola et al.* [1994] observe that the percolation threshold is more pronounced for the imaginary than for the real part of the mixture permittivity. That is, the threshold for abrupt change in the permittivity can be identified more reliably from ε_f'' curves than from ε_f' curves. Using these general findings, we can readily see from $\varepsilon_f''(f_a)$ curves in Figures 3b, 3d, and 3f that for sea foam the percolation threshold predicted by the PS rule (dashed lines) is, as expected from the theory, around $f_a = 70\%$. Also, as expected, it is more noticeable at 1.4 GHz than at 37 GHz because the dielectric contrast between seawater and air increases as frequency decreases (compare the y-axis values in Figures 3b, 3d, and 3f).

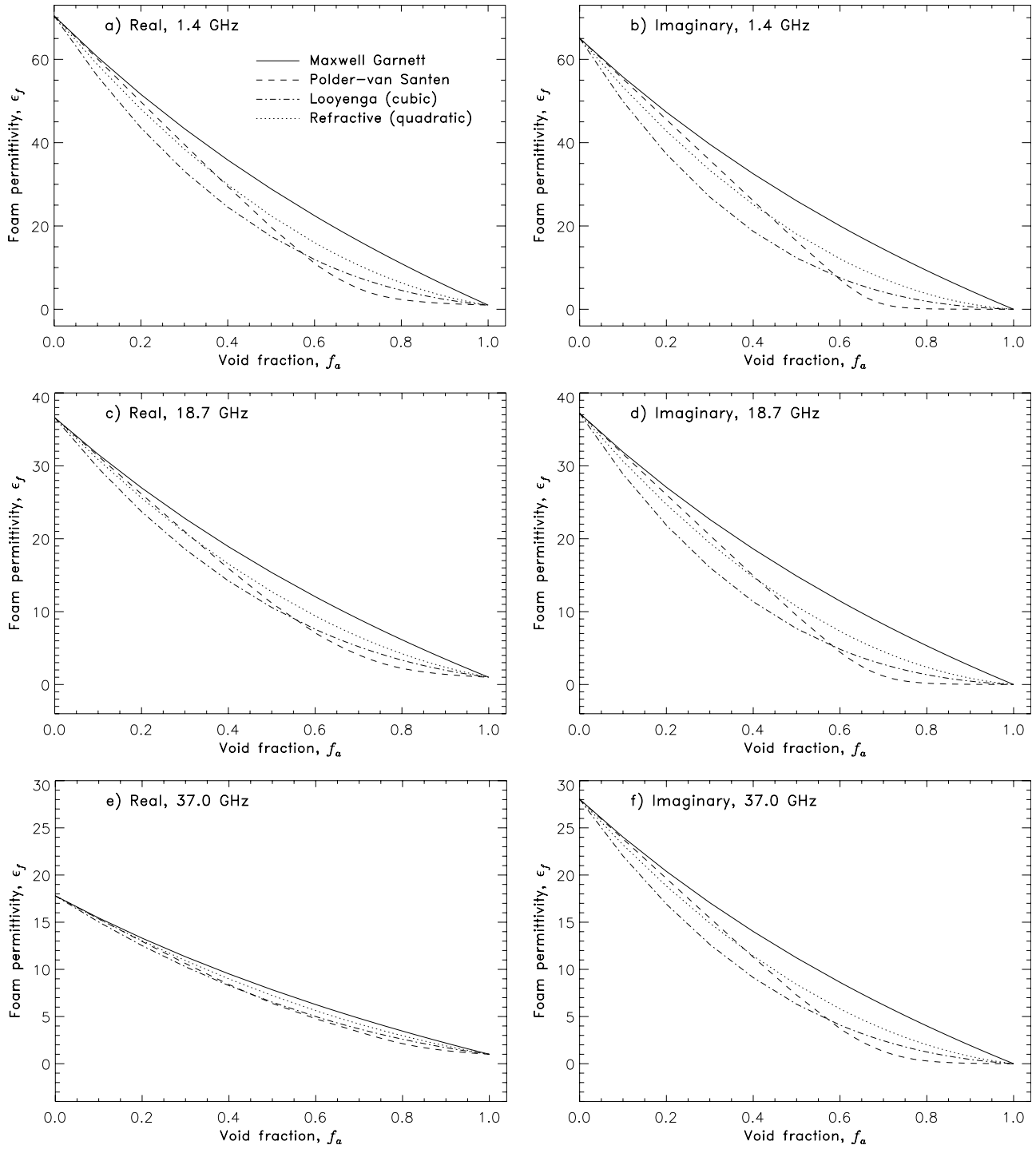

Figure 3. Foam permittivity as a function of foam void fraction obtained with four mixing rules: MG (solid line), PS (dashed line), Looyenga (dash-dot line), and Refractive (dotted line). (a and b) The real (ε'_f) and the imaginary (ε''_f) parts of foam permittivity at 1.4 GHz. (c and d) ε'_f and ε''_f at 18.7 GHz. (e and f) ε'_f and ε''_f at 37.0 GHz.

3.4. Limitation of the Classical Mixing Rules

[36] Though derived by strictly static analysis, the classical mixing rules are applicable to unsteady phenomena such as the sea foam (section 2.2) within the quasi-static approximation [*Choy*, 1999, section 3.3; *Sihvola*, 1999, p. 43]. The quasi-static limit is formulated as $\lambda/(2\pi) > a$, or equivalently $ka < 1$, where k and λ are the wavenumber and wavelength of the radiation and a is the size (usually the radius) of the inclusions [*Sihvola*, 1999, p. 151]. It can be achieved, therefore, either by considering small scatterers (the well-known Rayleigh limit with small a) or by considering low frequencies (the low frequency, or equivalently

Table 2. Dielectric Constant of Seawater Calculated With the Model of *Stogryn* [1997] at Microwave Frequencies and Fixed Sea Surface Temperature (20°C) and Salinity (34 psu)

F, GHz	λ_0, cm (in air)	$\mathrm{Re}\{\varepsilon\} \equiv \varepsilon'$	$\mathrm{Im}\{\varepsilon\} \equiv \varepsilon''$	λ[b], cm (in seawater)	ka at a = 1 cm[a]	k_0a at a = 1 cm[a]
1.4	21.4	70.43	65.06	2.55	2.5	0.294
6.8	4.4	62.53	34.14	0.56	11.25	1.428
10.7	2.8	53.52	36.73	0.38	16.55	2.244
18.7	1.6	36.60	37.21	0.26	24.2	3.927
23.8	1.3	28.98	35.00	0.23	27.3	4.833
37.0	0.8	17.79	28.03	0.19	33.1	7.757

[a]Size parameters ka and k_0a for large bubbles.
[b]$\lambda \cong \lambda_0/\sqrt{\varepsilon'}$.

the long wavelength, limit with low k). The representation of the quasi-static (i.e., temporal) limit in terms of spatial characteristics allows defining the low-frequency limit as the frequency at which attenuation by scattering is small compared to attenuation by absorption [*Tsang et al.*, 1985, p. 377]. Therefore the scattering in foam that we ignore in this study is an expression of the quasi-static limitation of the considered mixing rules. The estimates described below confirm this.

[37] In the formulation of the quasi-static approximation the radiation wavelength is not uniquely defined. It could be the wavelength in the environment, in the inclusions, or in the mixture [*Sihvola*, 1999, p. 151]. In Table 2, we present values for the size parameters ka and k_0a estimated using λ and λ_0 (wavelengths in seawater and in air, respectively) and a = 1 cm. In the worst-case scenario (ka for the shortest λ and the largest expected a), the low-frequency limit is violated at all frequencies for large bubbles. For smaller bubbles, e.g., a = 1 mm and 100 μm, the ka values decrease by one and two orders of magnitude, respectively. With this the low-frequency limit, thus the applicability of the classical mixing rules, is less severely violated for some frequencies and fully applicable for others, and this applicability gradually extends to higher and higher frequencies. For the smallest bubbles, the low-frequency limit holds true even for 37 GHz (ka = 0.3 for a = 100 μm).

[38] Since the scattering in foam is weak (section 2.3), we surmise that the worst-case scenario in Table 2 rarely plays out. This is explained with the bubble size distribution in sea foam [*Militskii et al.*, 1977; *Deane and Stokes*, 2002]: larger bubbles are much fewer (up to 10) than smaller ones (hundreds to thousands). As a result the contribution of the large bubbles to the scattering, though present, is not significant. The limitation introduced by the use of the classical mixing rules is mostly for higher frequencies (above 18 GHz) and is up to 15%, the scattering that we ignore in this study. The presented estimates can be further refined to take into account changes of k and λ within foam as its structure changes in time and space, but such analysis will be presented elsewhere.

3.5. Mixing Rules Selected for This Study

[39] Using the established limits for heterogeneous mixtures, we easily narrow down the number of available mixing rules potentially suitable for sea foam. Outside the limits defined by the MG and the PS rules (Figure 2b) are the Silberstein formula (linear law, long-dashed line) and the Lichtenecker formula (logarithmic law, dash-dot line). Previous experimental measurements and numerical investigations help us decide which of the remaining mixing rules (Table 1) merit further investigation for application to sea foam.

[40] Derived using the dipole moment of a single inclusion, MG is considered appropriate for diluted mixtures and has been observed to deviate from expected values in mixtures with high dielectric contrast and/or high volume fractions of the inclusions when the multipole interaction and multiple scattering are important [e.g., *Chew et al.*, 1990]. Applying it to bubble plumes with void fractions $\leq$20%, recent foam emissivity models use the MG rule in its supposed range of applicability [*Guo et al.*, 2001; *Chen et al.*, 2003; *Camps et al.*, 2005]. Yet, there is analytical [*Wu and Whites*, 2001; *Mallet et al.*, 2005] and experimental [*Koh*, 1992] evidence that in some cases the MG rule holds its accuracy for heterogeneous mixtures with higher density of the inclusions. For example, numerical results for touching air spheres arrayed in structures with different packing factors and embedded in dielectrically stronger material (analogous to sea foam) have shown close agreement with the MG predictions in the long-wavelength limit [*Datta et al.*, 1993, their Figure 2]. Such findings imply that the MG rule is able to handle not only high inclusion density, but also their close packing (e.g., from diamond to simple cubic to face-centered cubic). Perhaps these recent findings could explain the reasonable results obtained with earlier foam emissivity models [*Droppleman*, 1970; *Rosenkranz and Staelin*, 1972; *Wentz*, 1974], which have used the MG rule to obtain foam permittivity either for the full range (from 0 to 1) or for only high ($\geq$0.9) void fraction values. Thus, despite its expected limitations for densely packed mixtures, the MG rule classifies as an appropriate contender for use in foam studies.

[41] The PS and the CP formulae account to some extent for the multipole interaction at a higher density of inclusions by assigning to the particle surroundings the dielectric properties of the mixture, not those of the environment material alone [*Polder and Van Santen*, 1946; *Ulaby et al.*, 1986, Appendix E]. Being identical to the low-frequency limit of their respective exact formulae, which explicitly involve scattering terms [*Tsang et al.*, 1985, pp. 378–9 and pp. 474–5], the PS and CP mixing rules, as given in Table 1, offer implicit treatment of the scattering in dense media. As a result, the PS and the CP mixing rules have been successfully used for dense geophysical media [*Sihvola*, 1999]. Indeed, dielectric measurements of dry and wet snow in the 3 to 37 GHz range compare closely with predictions of PS formula [*Hallikainen et al.*, 1986] under low-frequency-limit conditions. Since at the frequencies of interest in our study absorption in foam dominates over scattering

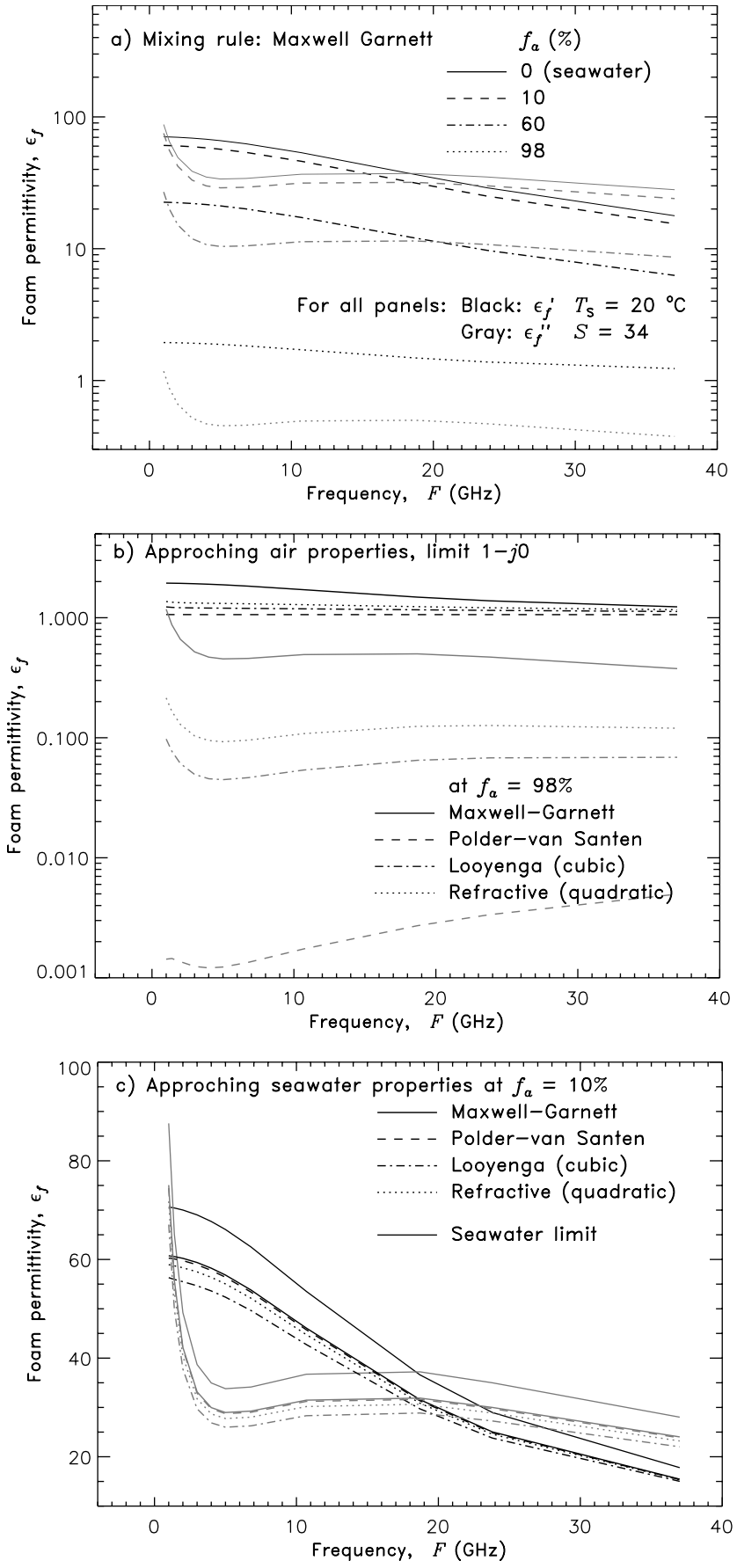
a) Mixing rule: Maxwell Garnett
f_a (%)
0 (seawater)
10
60
98
For all panels: Black: ϵ_f' T_S = 20 °C
Gray: ϵ_f'' S = 34
Foam permittivity, ϵ_f
Frequency, F (GHz)
b) Approching air properties, limit 1−j0
at f_a = 98%
Maxwell−Garnett
Polder−van Santen
Looyenga (cubic)
Refractive (quadratic)
c) Approching seawater properties at f_a = 10%
Seawater limit

Figure 4

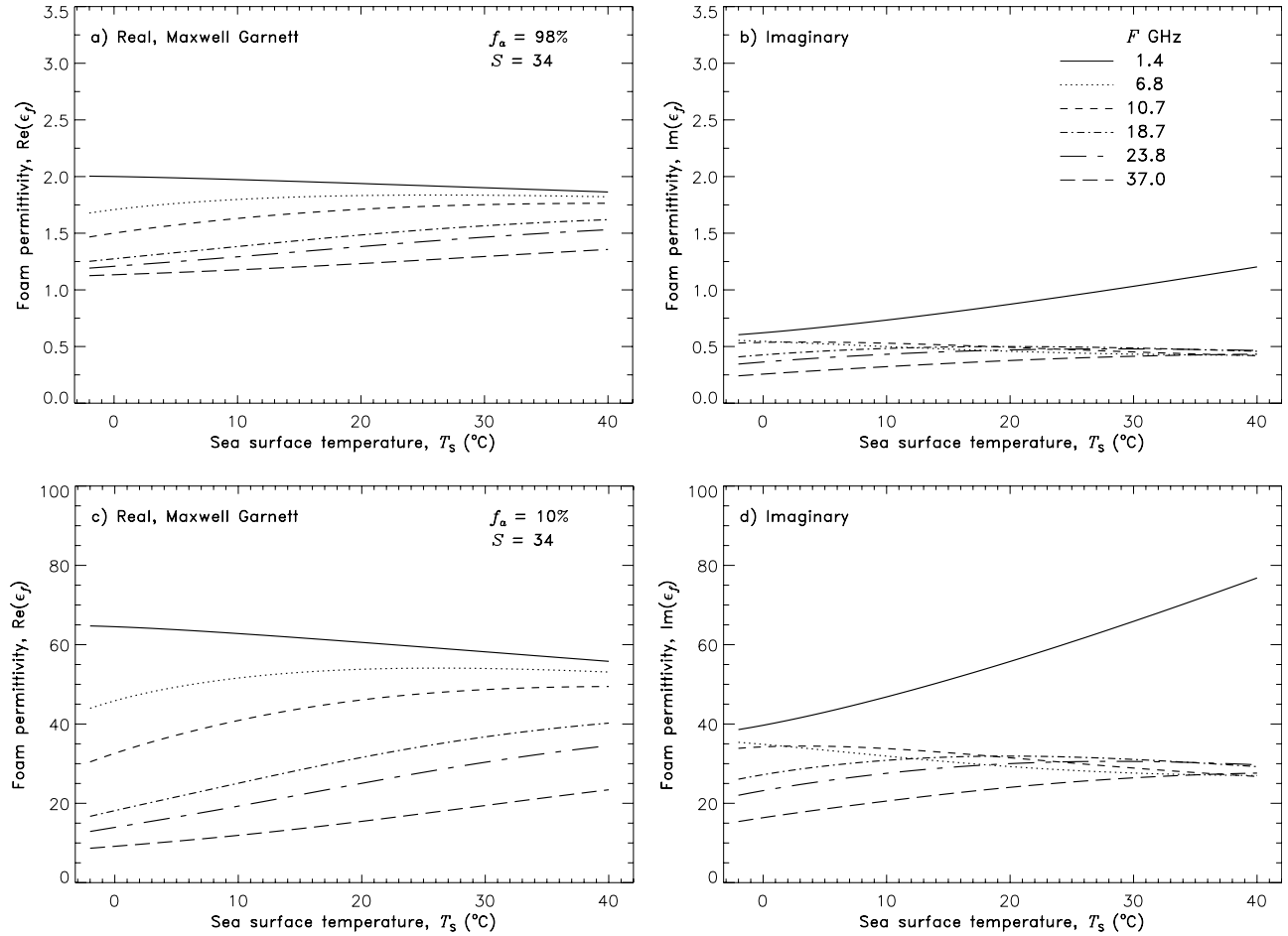

Figure 5. Foam permittivity, obtained with the Maxwell Garnett model, as a function of seawater temperature at various frequencies (see the legend) and fixed salinity (S = 34 psu). (a and b) Real and imaginary parts at void fractions f_a of 98% (dry foam). (c and d) Real and imaginary parts at void fractions f_a of 10% (wet foam).

(section 2.3), mixing rules resulting from the low-frequency-limit assumption are admissible.

[42] The Looyenga (cubic) model is a valuable contender for foam emissivity predictions because, among a suite of mixing rules (including the MG and the PS rules but not the Refractive law), it fits best with experimental data, especially at higher volume fractions (up to 35%) [*Looyenga*, 1965; *van Beek*, 1967, pp. 100–1].

[43] Finally, we also consider the Refractive (quadratic) model because it has been successfully used for heterogeneous mixtures comprising constituents with very different dielectric properties as is the case for the sea foam. *Gladstone and Dale* [1863, section II] find that the Refractive model gives "the nearest approximation to the truth" when comparing its predictions to experimental data for the refractive index (the square root of the dielectric constant) of a mixture of two liquids with refractive indices "very wide apart". The Refractive model has shown good agreement with experimental data when applied to obtain the dielectric constant of sea ice and dry soil [*Ulaby et al.*, 1986, Appendix E].

[44] Thus the permittivity models investigated here for obtaining the dielectric constant of sea foam are the Maxwell Garnett, Polder-Van Santen, Coherent potential, Looyenga, and Refractive models.

4. Results

[45] For the dielectric constant of seawater ε we use a double Debye model [*Stogryn*, 1997]. The seawater permittivity model of *Stogryn* [1997] is applicable for a frequency range of 5 to 100 GHz. Still, we use *Stogryn*, 1997 model

Figure 4. Foam permittivity, real (black lines) and imaginary (gray lines) parts, as a function of frequency at fixed seawater temperature (T_s = 20°C) and salinity (S = 34 psu). (a) Maxwell Garnett model at foam void fractions f_a of 98% (dotted lines), 60% (dash-dotted lines), and 10% (dashed lines). Seawater values are shown with solid lines. (b) At fixed f_a = 98% (dry foam) for four mixing rules Maxwell Garnett (solid line), Polder-Van Santen (dashed line), Looyenga (dot-dashed line), and Refractive (dotted line). (c) At fixed f_a = 10% (wet foam) for the same mixing rules as in Figure 4b. Seawater values are shown with thin solid line.

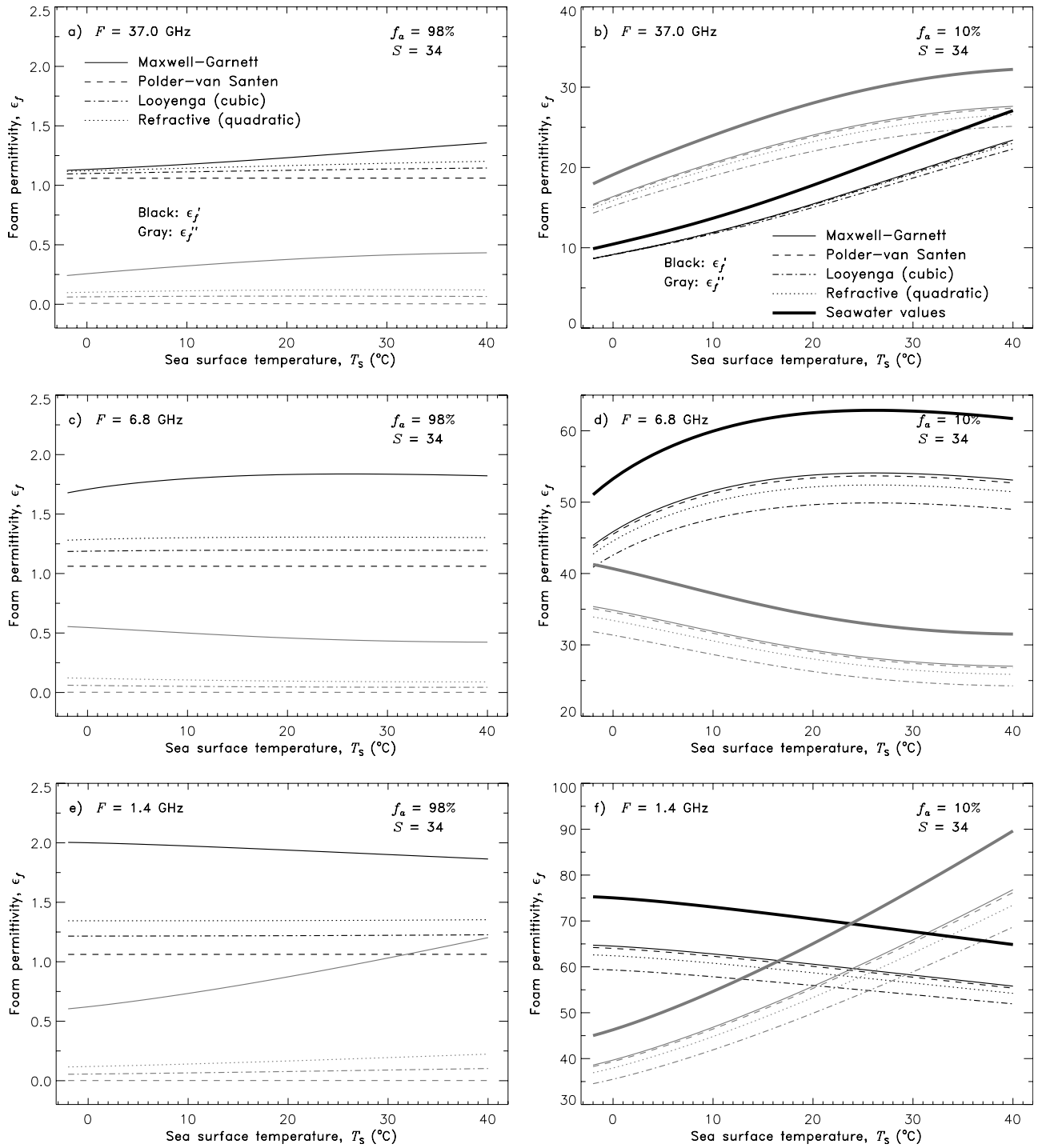

Figure 6. Foam permittivity, real (black lines) and imaginary (gray lines) parts, as a function of seawater temperature for four mixing rules: Maxwell Garnett (solid line), Polder-Van Santen (dashed line), Looyenga (dot-dashed line), and Refractive (dotted line) at fixed frequency and salinity ($S = 34$ psu). For wet foam (b, d, and f), the seawater values are shown with thick solid lines. (a and b) $f_a = 98\%$ and $f_a = 10\%$ at 37 GHz. (c and d) $f_a = 98\%$ and $f_a = 10\%$ at 6.8 GHz. (e and f) $f_a = 98\%$ and $f_a = 10\%$ at 1.4 GHz.

for frequencies down to 1 GHz, since its comparison to models applicable for L band (0.39 to 1.55 GHz) [*Klein and Swift*, 1977; *Meissner and Wentz*, 2004] reveal that its predictions of seawater permittivity at various salinities and water temperatures differ from L-band models by at most 2%. Table 2 lists the real and imaginary parts of seawater permittivity for the frequencies under consideration at SST of 20°C and salinity of 34 psu.

[46] Figure 3 depicts ε'_f and ε''_f as a function of the void fraction f_a at three frequencies (1.4, 18.7, and 37 GHz)

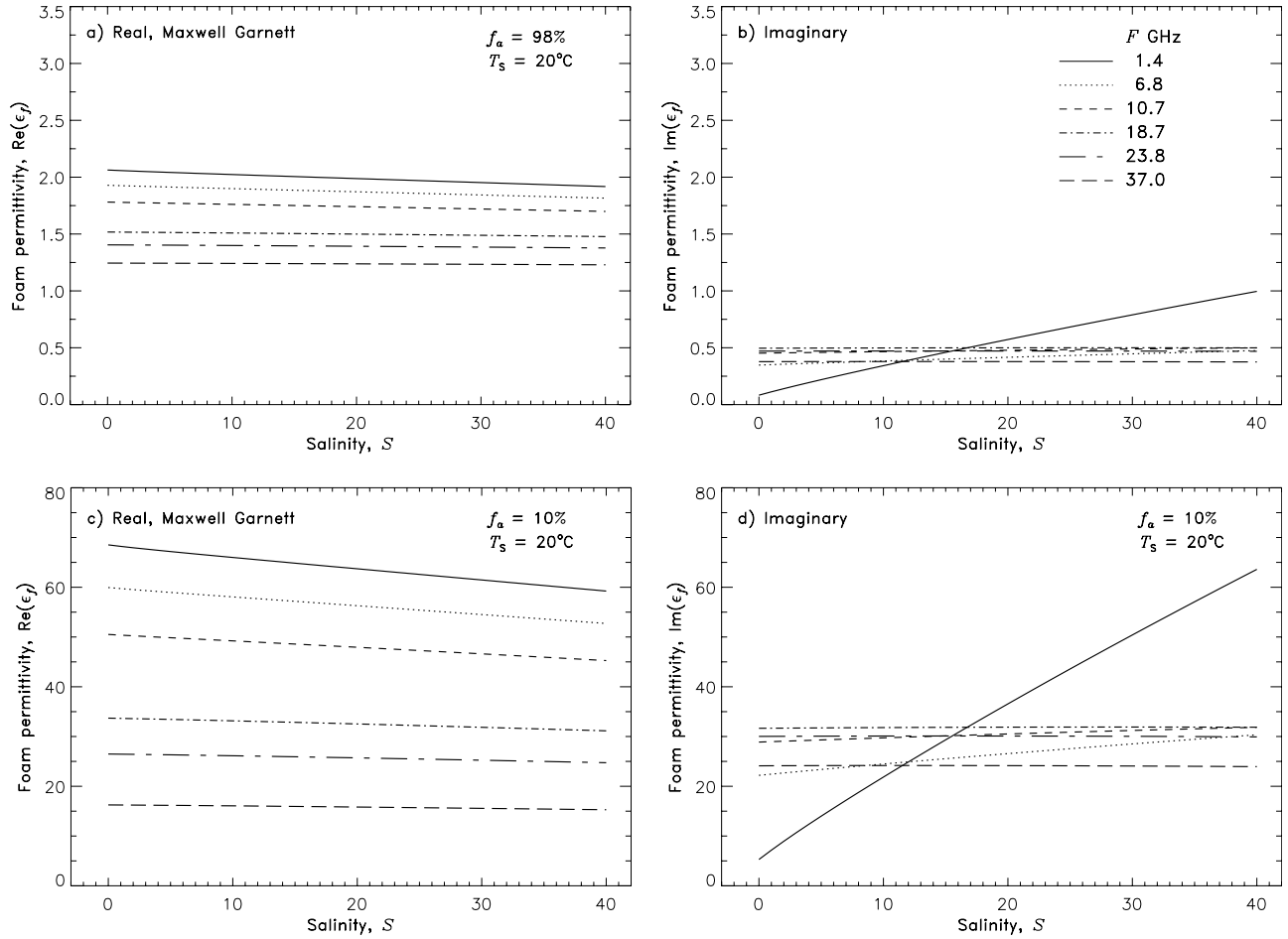

Figure 7. Foam permittivity, obtained with the Maxwell Garnett model, as a function of salinity at various frequencies (see the legend) and fixed seawater temperature (T_s = 20°C). (a and b) Real and imaginary parts at void fractions f_a of 98% (dry foam). (c and d) Real and imaginary parts at void fractions f_a of 10% (wet foam).

obtained with four mixing rules. (The reason for dropping the CP formula from further considerations is discussed in section 5.1.) We observe that the range of permittivity values allowed between the lower (PS) and upper (MG) bounds is frequency dependent. For ε'_f, the maximum variations allowed range from around 12 at 1.4 GHz to 1.5 at 37 GHz; for ε''_f, the allowed variations are from around 14 at 1.4 GHz to 5 at 37 GHz. Since we do not consider scattering losses explicitly (section 2.3), in the results ε''_f quantifies purely absorption losses and does not include scattering losses.

[47] While the dependence on the void fraction (Figures 2 and 3) is a characteristic of the foam itself as a dielectric medium, dependencies on the radiation frequency, F, the SST, T_s, and salinity, S, are "imposed" on the foamy mixtures by the dependence of the seawater dielectric constant on them. In this section, we focus our analysis on the major sea foam dependences for dry (f_a = 98%) and wet (f_a = 10%) foam obtained only with the Maxwell Garnett (MG) mixing rule for two reasons. First, the MG predictions represent the highest possible values of ε_f for various environmental (T_s and S) and observational (F) conditions (Figures 4a, 5 and 7). Second, comparisons of the MG predictions of ε_f to those obtained with the other mixing rules (Figures 4b–4c, 6, and 8) demonstrate that, though with some variations of the absolute ε_f values, the observations for all major dependencies remain essentially the same. The differences among the mixing rules' predictions and the insights gained from them are discussed in section 5.2. In Figures 4–8, the void fraction values representing dry and wet foam (98% and 10%) are chosen such as to avoid close clustering of the curves and demonstrate clearly the differences between the mixing rules.

[48] Figure 4a shows the frequency dependence $\varepsilon_f(F)$ as predicted with the MG rule for various void fraction values at fixed SST (T_s = 20°C) and salinity (S = 34 psu). The $\varepsilon_f(F)$ is weak for dry foam with f_a = 98% (dotted lines, black and gray colors for Re and Im parts, respectively). As air content in foam decreases to void fractions of 60% (dot-dashed lines) and 10% (dashed lines), the trend of $\varepsilon_f(F)$ strengthens and more closely resembles the frequency dependence of seawater permittivity (solid lines). The permittivity of wet foam depends strongly on the frequency, changing from O(60) at 1.4 GHz to O(15) at 37 GHz. Dry foam, containing a large amount of air, is nearly lossless with an imaginary part of around 0.2 for frequencies down to about 5 GHz. Though ε''_f increases faster for frequencies below 5 GHz, the relation $\varepsilon''_f < \varepsilon'_f$ still holds, rendering the dry foam a low

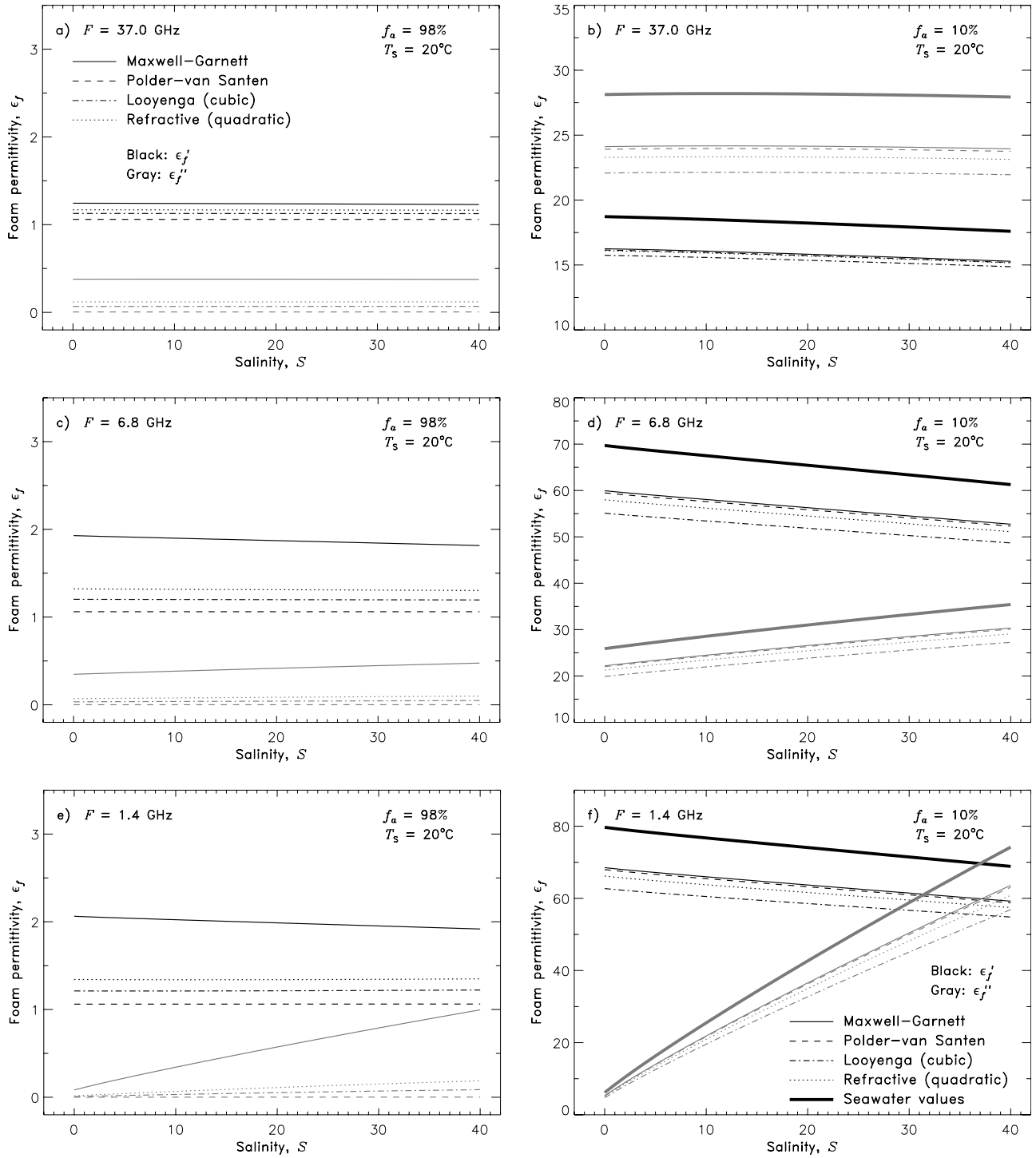

Figure 8. Foam permittivity, real (black lines) and imaginary (gray lines) parts, as a function of salinity for four mixing rules: Maxwell Garnett (solid line), Polder-Van Santen (dashed line), Looyenga (dot-dashed line), and Refractive (dotted line) at fixed frequency and seawater temperature (T_s = 20°C). For wet foam (b, d, and f), the seawater values are shown with thick solid lines. (a and b) f_a = 98% and f_a = 10% at 37 GHz. (c and d) f_a = 98% and f_a = 10% at 6.8 GHz. (e and f) f_a = 98% and f_a = 10% at 1.4 GHz.

loss medium at low frequencies. At f_a = 10%, ε_f' and ε_f'' are comparable indicating that wetter foam, as expected, is a more lossy medium. This is true already at f_a = 60% suggesting that the f_a range for dry, lossless foam is quite limited compared to that for wet, lossy foam.

[49] Figure 5 shows $\varepsilon_f(T_s)$ for dry (f_a = 98%) and wet (f_a = 10%) foam at various frequencies and fixed salinity (S = 34 psu). According to Figures 5a and 5b, the MG rule predicts weak dependence of ε_f' and ε_f'' on SST for dry foam at most frequencies (ε_f'' at 1.4 GHz is an exception). For wet

foam, Figures 5c and 5d establish that, though not especially strong, there is a noticeable dependence of ε'_f and ε''_f on SST resembling that of the seawater permittivity $\varepsilon(T_s)$, which is visualized for three frequencies in Figures 6b, 6d, and 6f with black (for ε') and gray (for ε'') thick solid lines. For all WindSat frequencies (from 6.8 to 37 GHz, Figures 5c and 5d) there is a steady increase of ε'_f with increasing SST. The rate of increase is higher at lower SST, up to 15°C. The imaginary part ε''_f shows weaker dependence on SST for WindSat frequencies with larger variations between frequencies at lower SST. At 1.4 GHz, the $\varepsilon'_f(T_s)$ trend is reversed compared to those of the other frequencies (i.e., a decrease of ε'_f with SST increasing) and $\varepsilon''_f(T_s)$ is exceptionally strong.

[50] Figure 7 shows $\varepsilon_f(S)$ for dry (f_a = 98%) and wet (f_a = 10%) foam at various frequencies and fixed SST (T_s = 20°C). For dry foam (Figures 7a and 7b), the MG mixing rule predicts barely noticeable dependence of ε'_f and ε''_f on S at all frequencies except 1.4 GHz. For wet foam (Figures 7c and 7d), $\varepsilon_f(S)$ is clearly seen for lower frequencies (below 10.7 GHz). As expected, it resembles that of the seawater permittivity $\varepsilon(S)$ (Figures 8b, 8d, and 8f, thick solid lines). For the WindSat range of frequencies (Figures 7c and 7d), $\varepsilon''_f(S)$ at 6.8 GHz is most noticeable, yet it is dwarfed by $\varepsilon''_f(S)$ at 1.4 GHz in accord with *Wilheit*'s [1978] findings that the salinity effect is most appreciable for frequencies below 5 GHz.

5. Discussion

[51] We use the results from section 4 to discuss and judge the suitability of the selected mixing rules for computing the dielectric constant of sea foam on the basis of three criteria: (1) how well a permittivity model deals with the full range of void fractions, (2) how a permittivity model behaves approaching the foam-air and foam-water boundaries, and (3) how the choice of a permittivity model affects estimates of emissivity and brightness temperature due to foam.

5.1. Applicability Over the Full Range of Void Fractions

[52] At any given void fraction value the MG and PS mixing rules establish a seemingly tight (and frequency dependent) range of possible values for foam permittivity (Figure 3 and section 4). Figures 2d, 2e, and 2f show how predictions of the selected mixing rules relate to the range of possible values at 18.7 GHz.

[53] The most conspicuous observation in Figure 2d for the CP mixing rule (dash-dots line) is the sharp change in the $\varepsilon_f(f_a)$ trend. For low void fractions both the real and imaginary (not shown) parts are slightly lower than the PS limit. For f_a > 20%, the real part becomes much larger than the upper limit set by the MG rule, while the imaginary part is much lower than the PS limit, both with trends inconsistent with the expected monotonic decrease as f_a increases. Obviously, the CP mixing rule in its low-frequency limit (scattering term ignored) will not model adequately the sea foam permittivity in macroscopic terms.

[54] The observed behavior is in strong contrast with the behavior of the PS rule despite the fact that both these mixing rules share similar approach of accounting for inclusion interactions and are successful in predicting the dielectric behavior of dense media (e.g., snow) in their low-frequency-limit forms. That is, while the PS mixing rule predicts consistently the dielectric behavior of both material-in-air ($\varepsilon_i/\varepsilon_e > 1$) and air-in-material ($\varepsilon_i/\varepsilon_e < 1$) mixtures, the CP rule gives consistent predictions only for the former case.

[55] Figures 2e and 2f show that above a specific void fraction value, approximately $f_a \geq 55\%$ for the cubic (Looyenga) and $f_a \geq 35\%$ for the quadratic (Refractive) laws, the predictions of these two mixing rules are above the lower limit of the allowable ε_f set by the PS rule. Since according to the EMT the more we know about a mixture the closer its bounds come together (section 3.2), we expect the true values for ε_f to fall somewhere between the MG and PS limits. Following this supposition, we interpret the results for the cubic and quadratic laws as an improvement in the foam permittivity predictions at higher void fractions compared to the established upper and lower values. Figure 3 illustrates that these observations hold for both ε'_f and ε''_f values at different frequencies. For the wet foam (low f_a values) at the bottom of a foam layer, the PS mixing rule continues to predict the lowest values. While the Looyenga formula is significantly lower than the PS limit, but still well above the HS lower bound (solid gray line in Figure 2a), the quadratic law differs from the PS rule by at most 4% for ε'_f and up to 7% for ε''_f at any of the considered frequencies.

[56] In summary, guided by the upper and lower limits for the permittivity of sea foam as shown in Figure 2, we exclude from further consideration the CP mixing rule and expect all other mixing rules to give consistent predictions for the sea foam permittivity. The Refractive model is expected to outperform two of the other models because it improves ε_f predictions over a larger range of void fractions compared to the Looyenga rule and it differs only slightly from the PS rule in the low-fractions end.

5.2. Sea Foam Dependencies at the Boundaries

[57] Missing experimental data to confirm the inferences from Figures 2 and 3 on the applicability of the mixing rules over the full range of void fractions, we can use the major sea foam dependencies as another way to judge the suitability of those rules to sea foam. Formally, at the end points of the void fraction range all mixing formulae correctly calculate the air and seawater permittivities at the air-foam and foam-water interfaces: $\varepsilon_f = \begin{cases} 1 & @f_a = 1 \\ \varepsilon & @f_a = 0 \end{cases}$. We can expect, therefore, dry foam (having a small amount of seawater) to behave more like air with ε_f approaching $1 - j0$ and wet foam to behave more like seawater with ε_f approaching $\varepsilon(F, T_s, S)$. As hinted by the slopes of the $\varepsilon_f(f_a)$ curves in Figures 2 and 3, the different mixing rules will attain the boundary conditions with a different rate. Observing which mixing rule reproduces air and seawater behaviors plausibly when approaching the void fraction extrema, we have a second criterion for evaluating the mixing rules suitability. Though admittedly weak, in the absence of any experimental data for ε_f, this criterion provides a qualitative support for the conclusions of this study.

[58] Figure 4b for dry foam (f_a = 98%) shows that of all mixing rules, the PS predictions (black and gray dashed

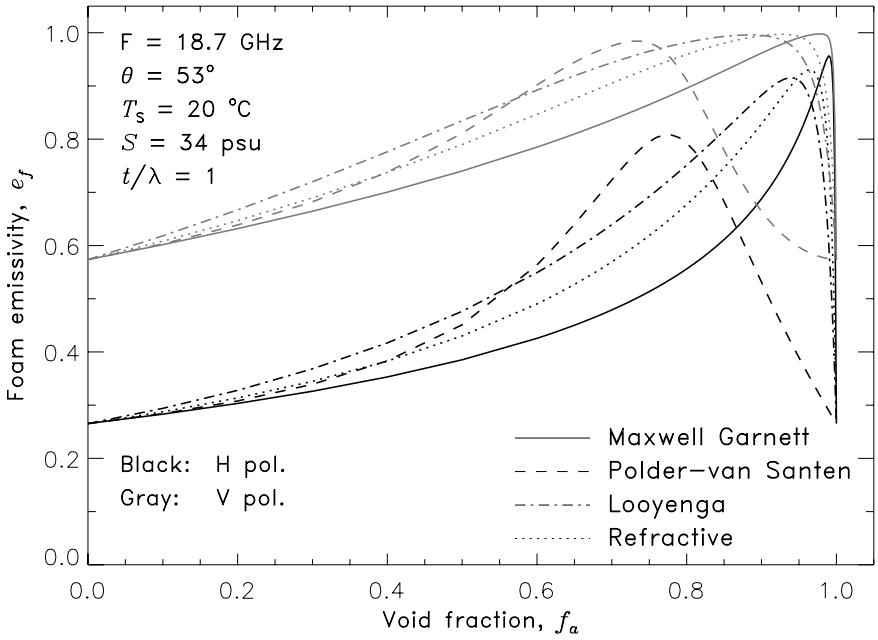

Figure 9. Foam emissivity as a function of void fraction obtained using four mixing rules: Maxwell Garnett (solid lines), Polder-Van Santen (dashed lines), Looyenga (dot-dashed line), and Refractive (dotted line) for 18.7 GHz, H (black lines) and V (gray lines) polarizations. The model parameters are incidence angle θ of 53°, sea surface temperature T_s of 20°C, salinity S of 34 psu, and foam thickness of one wavelength, $t/\lambda = 1$.

lines) reproduce the lossless and frequency-independent behavior of air most closely. Concluding section 3.3, we noted that the PS rule places the percolation threshold for sea foam at $f_a \approx 70\%$. According to the definition of the percolation threshold, at this critical f_a value the behavior of the sea foam mixture sharply switches from that of the environment (seawater) to that of the inclusions (air). Thus, according to the PS rule, the sea foam exhibits air-like behavior already at $f_a \geq 70\%$. However, it is accepted in the EMT theory that at $f_c \approx 1/3$ the PS formula predicts an overly high percolation threshold for material-in-air mixtures [*Choy*, 1999, p. 13]; conversely, $f_c \approx 2/3$ is too low for air-in-material mixtures like the sea foam. We infer, therefore, that with the PS rule the sea foam permittivity attains the air characteristics prematurely.

[59] Meanwhile, in Figure 4b the MG rule features the highest ε''_f values and its ε'_f values have the most noticeable frequency dependence compared to all other rules. According to the MG rule predictions, even at this high air content in the sea foam (f_a = 98%), the typical seawater features continue to characterize the mixture because the percolation threshold for the MG rule is pushed to f_c = 100%. While extreme percolation thresholds are not forbidden and theoretically f_c values could be anywhere between 0% and 100% [*Landauer*, 1978 cited by *Sihvola et al.*, 1994], the behavior predicted by the MG rule is not likely since most real-life f_c values tend to be low [*Sihvola*, 1999, p. 230]. We surmise, therefore, that for dry foam the intermediate ε_f values predicted by the cubic and quadratic laws in Figure 4b are the more plausible ones.

[60] For wet foam at f_a = 10%, Figure 4c reveals that $\varepsilon_f(F)$ predictions from the MG and PS rules are the closest to the seawater values $\varepsilon(F)$. The Looyenga law places the ε_f values the farthest from those of seawater. The Refractive model, being slightly lower than the MG and the PS models yet above the Looyenga model, represents intermediate values. Combining this observation with the behavior revealed in Figure 4b for dry foam, we can reasonably state that on the basis of $\varepsilon_f(F)$ dependence, the Refractive mixing rule seems to be the most acceptable when approaching both boundaries.

[61] Analogous analyses of the $\varepsilon_f(T_s)$ and $\varepsilon_f(S)$ dependences in Figures 6 and 8 lead to the same conclusion. The MG rule, not reaching its percolation threshold until f_a = 100%, predicts the strongest dependences on T_s and S for dry foam at f_a = 98. Passing its percolation threshold at f_a = 70%, the PS rule predicts air-like trends for $\varepsilon_f(T_s)$ and $\varepsilon_f(S)$ over the entire high-void-fraction end of the f_a range. The cubic and the quadratic laws predict intermediate values. For wet foam, both the MG and the PS rules are closest to the seawater values, the cubic law is the farthest, and the quadratic law, placed closer to the MG and PS predictions, provides intermediate values.

[62] Thus, the analysis of foam permittivity dependences on F, T_s, and S shows that approaching the boundaries the Refractive model consistently predicts the expected air-like and seawater-like behavior of sea foam more plausibly than the MG, PS, and cubic models.

5.3. Impact on Foam Emissivity

[63] Since the foreseen application of this investigation of foam permittivity is its use to compute foam emissivity and the brightness temperature due to foam (section 1), we evaluate the impact of the various mixing rules on these quantities. The foam emissivity model, used for this analysis, combines the incoherent approach given by *Ulaby et*

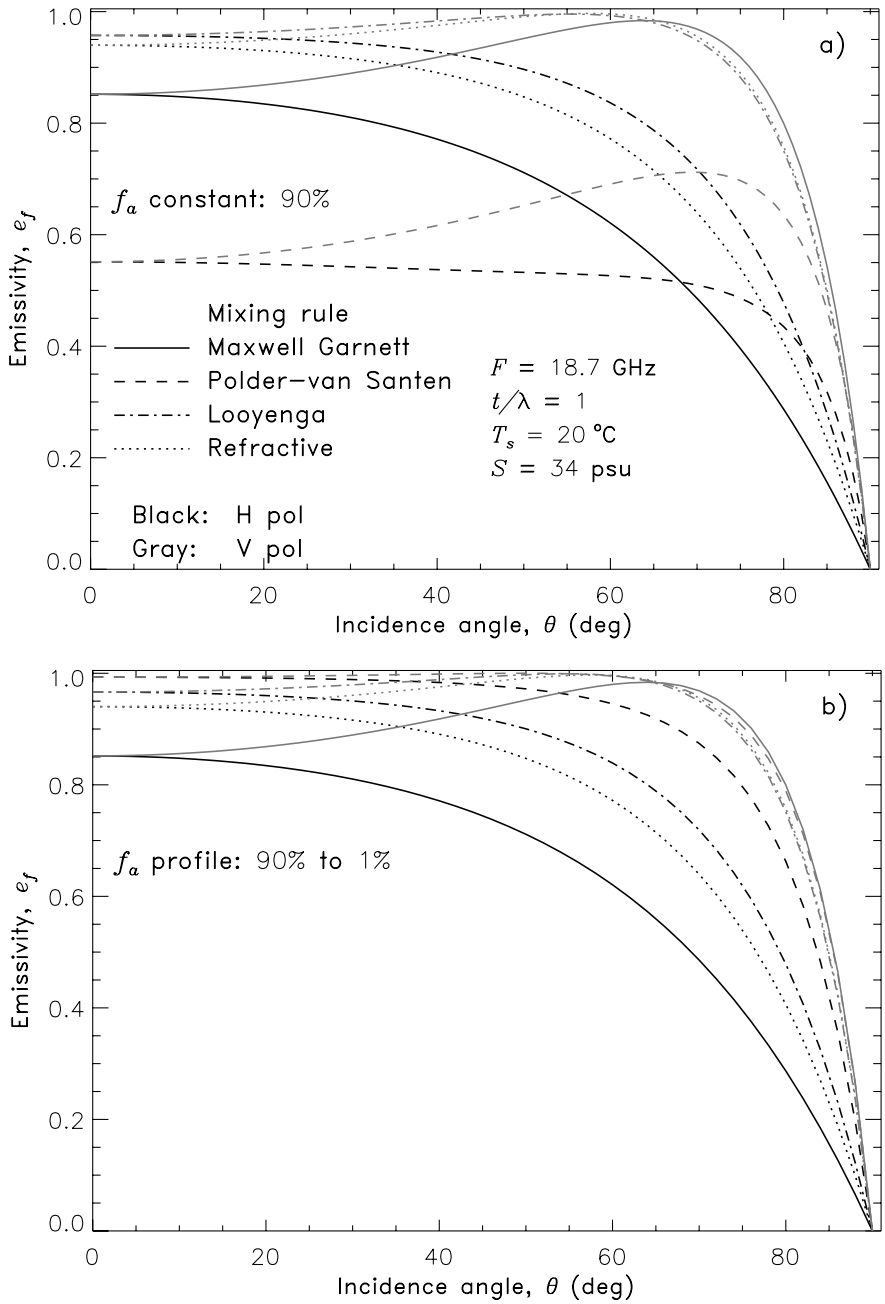

Figure 10. Foam emissivity as a function of incidence angle for four mixing rules; all notations as in Figure 9.

al. [1986, equation (18.41)] with a void fraction, thus dielectric, profile. The model is in terms of foam macroscopic characteristics, void fraction f_a and layer thickness t. This approach is more suitable for weakly scattering sea foam and avoids the emissivity oscillations as a function of foam thickness observed by the similar but not identical model of *Droppleman* [1970]. When run with an f_a profile constant in foam depth (constant f_a), the model replicates the incoherent approach results of *Ulaby et al.* [1986, their figures 18.27 and 18.28]; otherwise, it accounts for the vertical dielectric changes following an exponential void fraction profile (f_a profile).

5.3.1. The Effect of Mixing Rule Choice

[64] For any of the considered frequencies, exemplified in Figure 9 with results for 18.7 GHz, the choice of the mixing rule used for calculating the foam dielectric constant leads to quite different e_f values for void fractions above 40%. At a constant f_a value, e.g., f_a = 95% as *Droppleman* [1970] has suggested, e_f ranges from about 0.39 to 0.91. Figure 10a illustrates this point for the full range of incidence angles at a constant void fraction of 90%.

[65] If the void fraction of the foam is a set, well determined value, its use with each of the mixing rules to obtain foam emissivity will show unambiguously which permittivity model performs better. Figure 11 illustrates this

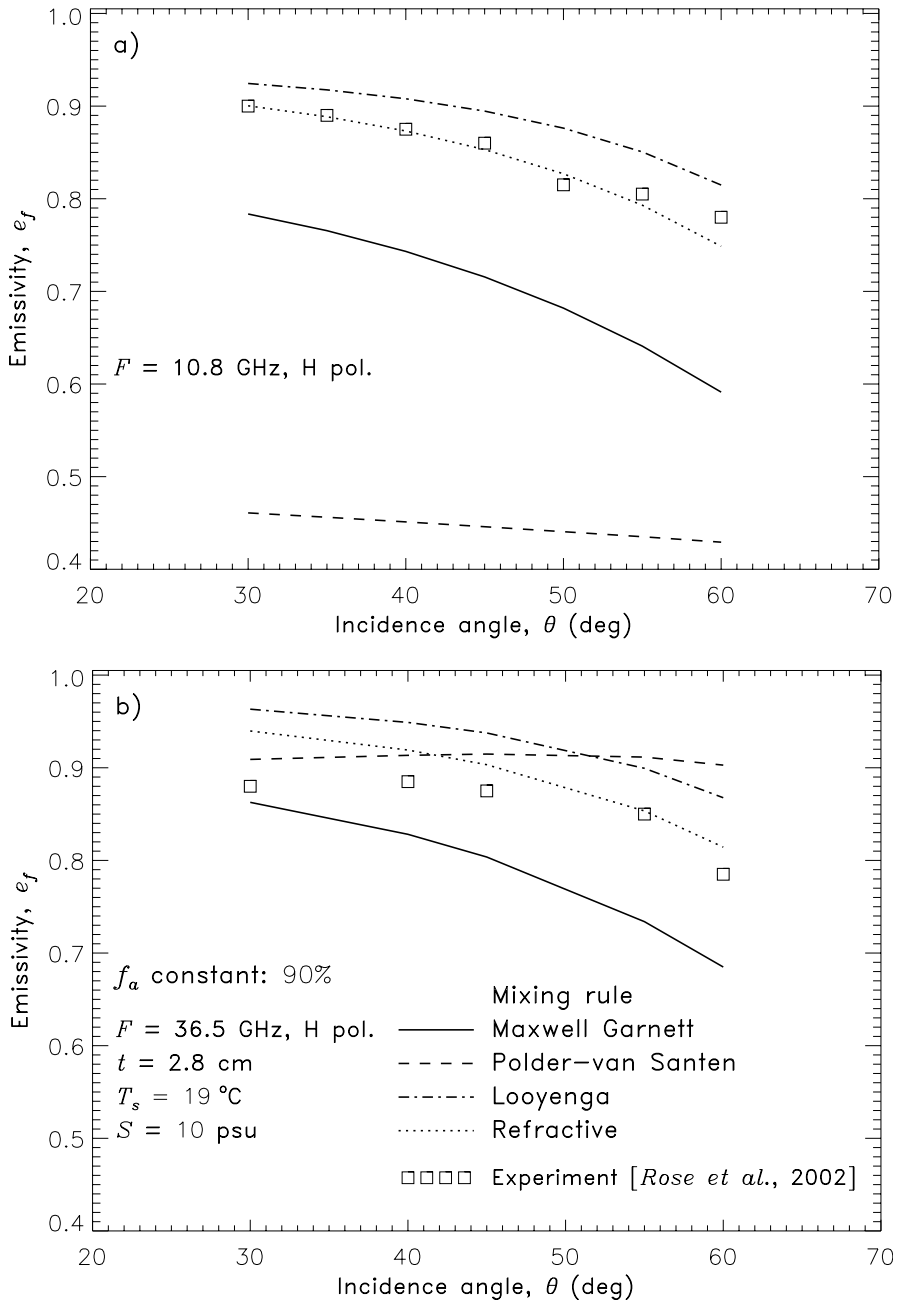

Figure 11. Foam emissivity as a function of incidence angle obtained using four mixing rules: Maxwell Garnett (solid lines), Polder-Van Santen (dashed lines), Looyenga (dot-dashed line), and Refractive (dotted)–compared to experimental (open squares) data at void fraction f_a = 90% for (a) 10.8 GHz, horizontal (H) polarization and (b) 36.5 GHz, H. The model parameters match those of the experimental data: T_s = 19°C, S = 10 psu, foam thickness t = 2.8 cm.

by comparing e_f computed with the four mixing rules to experimental e_f data provided by *Rose et al.* [2002] at 10.8 GHz and 36.5 GHz, with foam thickness of approximately 2.8 cm, water temperature of 19°C, and salinity of 10 psu. We represent the experimental void fraction with f_a = 90%, the mid-point between measured and expected f_a values [*Rose et al.*, 2002, p. 2623], used also by *Chen et al.* [2003]. For 10.8 GHz, H polarization (a), the predictions obtained with the Refractive model (dotted line) are in good agreement with the measurements (symbols), while the MG and PS rules (solid and dashed lines, respectively) significantly under-estimate e_f and the Looyenga model yields higher e_f. For 36.5 GHz (b), both the Refractive and the PS models are close to the experimental results, while the MG and Looyenga models still under- and over-predict e_f, respectively. For V polarization, similar considerations are less satisfactory, but reasonable. Thus, at the specific experimental set-up represented with f_a = 90%, the foam emissivity measurements validate the Refractive model as performing more consistently than the other mixing rules.

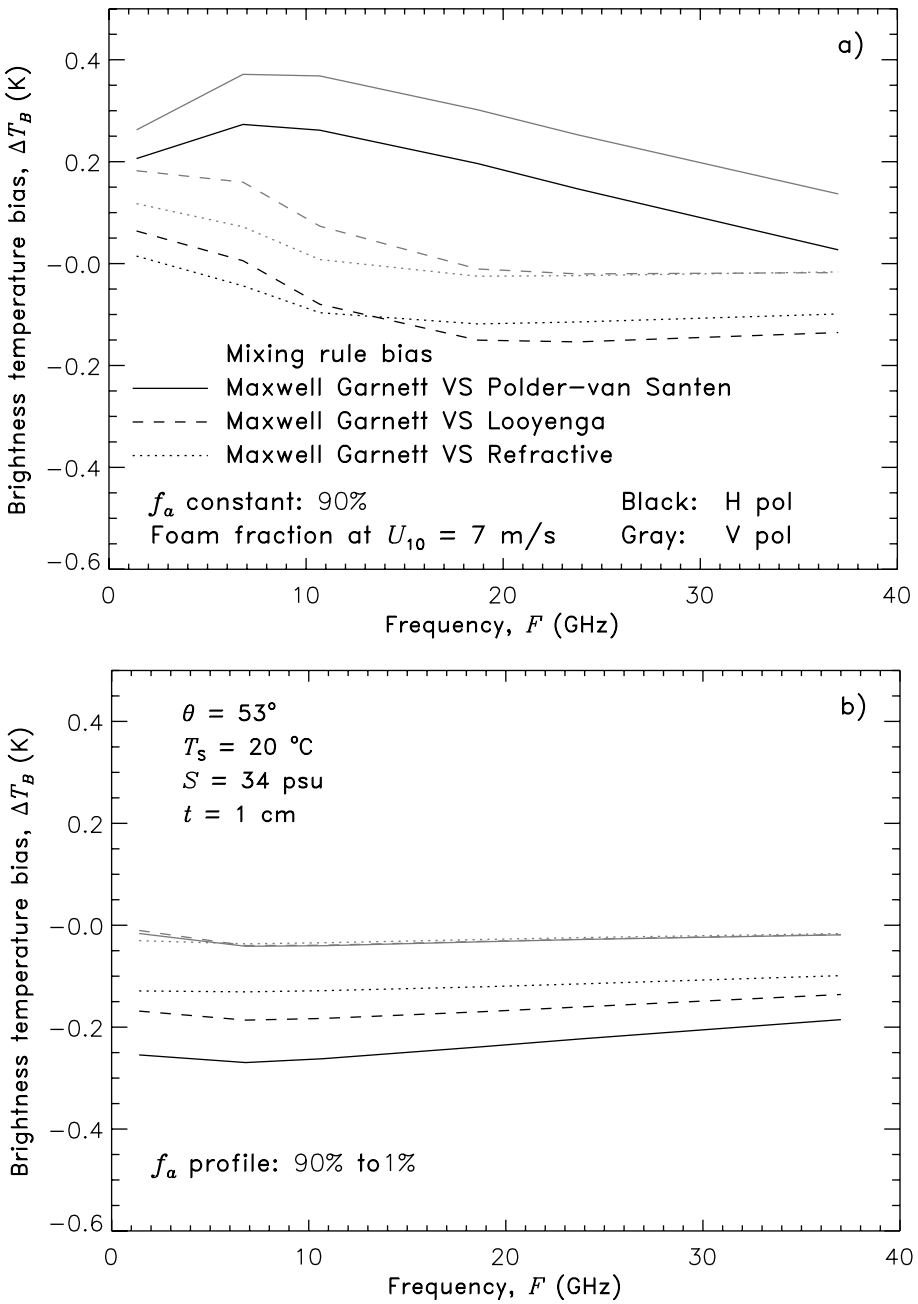

Figure 12. Bias in brightness temperature due to foam as a function of frequency representative for whitecap coverage under 7 m/s wind speed if Polder-Van Santen (solid lines), Looyenga (dashed lines), or Refractive (dotted lines) models are chosen instead of the Maxwell Garnett model. The modeling parameters are as in Figure 9, except the foam layer thickness, which is fixed at 1 cm for all frequencies. (a) Constant void fraction f_a = 90%. (b) Void fraction profile, f_a from 90% to 1%.

[66] Figure 12a illustrates the impact of the mixing rule choice on the brightness temperature due to foam. For various frequencies and polarizations with all other model parameters the same except for the mixing rule, biases of up to 0.4 K are introduced at foam coverage W associated with wind speed of 7 m/s, i.e., $\Delta T_B = W.\Delta e_f.T_s$ where $\Delta e_f = e_{fMG} - e_{fX}$ with X standing for any of other mixing rules. These biases increase ten-fold, up to 4 K, for wind speed of 14 m/s. Smaller biases are observed if the choice is between the Looyenga and the MG models (dashed lines) because Looyenga mixing rule brings the dielectric constant values closer to those of the MG rule (Figure 2e). By the same token (Figure 2f), the choice between the Refractive and the MG models leads to even smaller biases (dotted lines in Figure 12a). Still, uncertainties of this scale, introduced in a geophysical model via the choices in modeling the foam permittivity and the corresponding foam emissivity, would corrupt the accuracy of wind vector retrievals.

5.3.2. The Effect of Void Fraction Modeling

[67] Our review (section 2.2) has shown that foam is more accurately characterized with a void fraction profile in foam depth instead of a constant value. A change of the fixed constant value of f_a = 90% to a profile of the void fraction from 90% to 1% reduces the sensitivity of the foam emissivity model to the choice of a permittivity model with all other parameters the same (Figure 10b). Close examination of Figures 10a and 10b shows that at 18.7 GHz this is largely due to the increase of the e_f values obtained with the PS mixing rule (dashed lines), whereas the angular dependencies predicted with the MG rule (solid lines) are quite robust with respect to the choice of f_a as a constant or as a profile. The Looyenga and Refractive models (dash-dotted and dotted lines, respectively) change only slightly, leaving the PS model as the more sensitive one to the void fraction modeling.

[68] When void fraction is modeled as a profile instead of a constant value, the preference of any other mixing rule over the MG rule does not introduce T_B biases (Figure 12b) larger than 0.05 K under 7-m/s winds (0.5 K under 14-m/s wind) for V polarization at any frequency (gray lines). Some biases, around 0.2 K and 2 K under winds of 7 m/s and 14 m/s, respectively, still remain for H polarization (black lines). Inter-comparison of Figures 12a and 12b shows that the brightness temperature biases due to the choice of a mixing rule are less frequency dependent when a void fraction profile is used.

5.3.3. Void Fraction as a Tuning Parameter

[69] The high sensitivity of the e_f model to the mixing rule choice at a fixed void fraction persists when increasing f_a from 90% to 95% or 98% (Figure 9). Different tendencies are observed in the case of void fraction profile: if the upper value of the f_a profile is different (95% or 98% instead of 90%), the angular dependences $e_f(\theta)$ obtained with different mixing rules cluster more closely, usually at higher e_f values. That is, the wider the range of values covered by the void fraction profile, the less vulnerable the foam emissivity model is to the choice of a mixing rule. Variations of the lower value of the f_a profile, from 1% up to 40%, invoke negligible changes in the trends depicted in Figure 10. This implies that the high void fraction value, be it a constant f_a or an upper point in a f_a profile, is the dominant parameter influencing the dielectric profile and the corresponding emissivity.

[70] What is the realistic maximum void fraction value that characterizes foam in the open ocean? A wide range of maximum f_a values emerges from the available experimental observations, from 99–90% in radiometric to less than 90% in oceanographic measurements (sections 2.2 and 2.3). Most likely this value varies with the wind speed and the temporal evolution of the whitecaps from formation to decay. This implies that the maximum void fraction value could be used as a tunable parameter to express the emissivity from different foam layers in the ocean, at least until more experimental information for foam layers in open ocean becomes available. Using the maximum f_a as a tuning parameter would be analogous to the tuning of the models, which include scattering explicitly, via the choice of bubble radius and wall thickness [*Raizer and Sharkov*, 1981; *Chen et al.*, 2003, their section II].

[71] The possibility for tuning f_a, however, may lead to the choice of an inappropriate mixing rule. Left to an arbitrary choice of the maximum void fraction, each mixing rule can be tuned to eventually match the experimental data. Our analysis here provides some guidance to resolve this issue as it points to the Refractive mixing rule as the one that matches the available experimental data without, or with the least amount of, tuning.

6. Conclusions

[72] We have presented an investigation of the applicability of a suite of mixing rules for obtaining the dielectric constant of sea foam, ε_f, and the corresponding foam emissivity, e_f, namely, the Maxwell Garnett (MG), Polder-Van Santen (PS), Coherent potential (CP), Looyenga (cubic) and Refractive (quadratic) formulae. Discarding the CP rule as unsuitable (section 5.1 and Figure 2d), we use four mixing formulae to predict the permittivity of the sea foam ε_f and systematically document its main dependences on environmental and observational parameters, namely, the dependence on void fraction, $\varepsilon_f(f_a)$, on radiation frequency, $\varepsilon_f(F)$, on SST, $\varepsilon_f(T_s)$, and on salinity, $\varepsilon_f(S)$ (section 4 and Figures 3–8). To further examine the suitability of the permittivity models for computing ε_f, the performance of each mixing rule is evaluated on the basis of three criteria: (1) how well a permittivity model deals with a wide range of void fractions (section 5.1), (2) how a permittivity model behaves approaching the foam-air and foam-water boundaries (section 5.2), and (3) how the choice of a permittivity model affects estimates of emissivity and brightness temperature due to foam (section 5.3). The conclusions are as follows.

[73] All four permittivity models provide reasonable predictions for ε_f within the seemingly tight range of expected values established by the MG and PS rules (section 5.1). As an upper limit, the MG rule would provide the highest possible values for ε_f. Since according to the effective medium theory the true ε_f values should fall between the limits established by the MG and the PS rules (section 3.2), both the cubic (Looyenga) and quadratic (Refractive) models offer some improvement at higher void fractions. Further analysis (sections 5.2 and 5.3) shows that the Refractive law consistently predicts more plausible behavior and more acceptable estimates of foam emissivity as compared to the predictions of the other formulae. Overall, at microwave frequencies from 1 GHz to 37 GHz the recommended suitability of the considered mixing rules for obtaining the dielectric constant of sea foam floating on the ocean surface over the full range of possible void fractions ranks, from best to worst, as follows: (1) Refractive (quadratic) model; (2) Looyenga (cubic) model; (3) Maxwell Garnett model; (4) Polder-Van Santen model. An important finding of this study is that the sensitivity of a foam emissivity model, and the respective estimates of the brightness temperature due to foam, to the choice of a permittivity model significantly decrease if a void fraction (thus dielectric) profile is used instead of a constant f_a value.

[74] The limitation of the classical mixing rules rises from their quasi-static character. An expression of this limitation is the amount of scattering in the sea foam (section 3.4). Review of experimental and modeled results shows that the

scattering in foam is weak (section 2.3) and we ignore it in this study. The expected limitation of the mixing rules, therefore, is some underestimation of ε_f, much less, if at all, at lower frequencies (below 10 GHz) and no more than 15% at higher frequencies (above 18 GHz).

[75] Heeding the statement of the effective medium theory that no classical mixing rule can provide the true values for the permittivity of a mixture, the presented study serves mostly as a general guide when choosing a permittivity model for the sea foam. Measurements of ε_f over the full range of void fractions would improve its empirical parameterization and prediction. Numerical simulations of foamy mixtures with the FDTD method [*Kärkkäinen et al.*, 2000] could provide a foam-specific parameterization for the $\varepsilon_f(f_a)$ relation and further refine predictions of foam permittivity.

[76] **Acknowledgments.** This study was sponsored by the Office of Naval Research. The author thanks Gene Poe, Richard Cember, Ian Adams, and Bill Johnston for valuable suggestions and comments on the manuscript. The constructive critique of anonymous reviewers has markedly improved the initial manuscript.

References

Adamson, A. W. (1997), *Physical Chemistry of Surfaces*, 784 pp., John Wiley & Sons, New York.

Baldy, S. (1988), Bubbles in the close vicinity of breaking waves: Statistical characteristics of the generation and dispersion mechanism, *J. Geophys. Res.*, *93*, 8239–8248.

Bettenhausen, M. H., C. K. Smith, R. M. Bevilacqua, N.-Y. Wang, P. W. Gaiser, and S. Cox (2006), A nonlinear optimization algorithm for WindSat wind vector retrievals, *IEEE Trans. Geosci. Remote Sens.*, *44*, 597–610.

Blanchard, D. C., and A. H. Woodcock (1957), Bubble formation and modification in sea and its meteorological significance, *Tellus*, *9*, 145–158.

Bordonskiy, G. S., et al. (1978), Spectral characteristics of the emissivity of foam formations, *Izv. Atmos. Oceanic Phys.*, *14*, 464–469.

Camps, A., et al. (2005), The emissivity of foam-covered water surface at L-band: Theoretical modeling and experimental results from the FROG 2003 field experiment, *IEEE Trans. Geosci. Remote Sens.*, *43*, 925–937.

Chen, D., L. Tsang, L. Zhou, S. C. Reising, W. E. Asher, L. A. Rose, K.-H. Ding, and C.-Te Chen (2003), Microwave emission and scattering of foam based on Monte Carlo simulations of dense media, *IEEE Trans. Geosci. Remote Sens.*, *41*, 782–790.

Chew, W. C., J. A. Friedrich, and R. Geiger (1990), A multiple scattering solution for the effective permittivity of a sphere mixture, *IEEE Trans. Geosci. Remote Sens.*, *28*, 207–214.

Choy, T. C. (1999), *Effective Medium Theory: Principles and Applications*, 193 pp., Oxford Univ. Press, New York.

Dahl, P., and A. Jessup (1995), On bubble clouds produced by breaking waves: An event analysis of ocean acoustic measurements, *J. Geophys. Res.*, *100*, 5007–5020.

Datta, S., C. T. Chan, K. M. Ho, and C. M. Soukoulis (1993), Effective dielectric constant of periodic composite structures, *Phys. Rev. B*, *48*(20), 14,936–19,943.

De Loor, G. P. (1965), Dielectric properties of heterogeneous mixtures with a polar constituent, *Appl. Sci. Res.*, *Section B*(11), 310–320.

De Loor, G. P. (1983), The dielectric properties of wet materials, *IEEE Trans. Geosci. Remote Sens.*, *GE-21*(3), 364–369.

Deane, G. B., and M. D. Stokes (2002), Scale dependence of bubble creation mechanisms in breaking waves, *Nature*, *418*, 839–844.

Dombrovskiy, L. A. (1979), Calculation of thermal radio emission from foam on the sea surface, *Izv. Atmos. Oceanic Phys.*, *15*, 193–198.

Dombrovskiy, L. A. (1982), Absorption and scattering of microwave radiation by spherical water shells, *Izv. Atmos. Oceanic Phys.*, *17*, 238–241.

Droppleman, J. (1970), Apparent microwave emissivity of sea foam, *J. Geophys. Res.*, *75*, 696–698.

Ellison, W. J., A. Balana, G. Delbos, K. Lamkaouchi, L. Eymard, C. Guillou, and C. Prigent (1996), Study and measurement of the dielectric properties of sea water, Final report, European Space Agency.

Fairall, C. W., E. F. Bradley, J. S. Godfrey, G. A. Wick, J. B. Edson, and G. S. Young (1996), Cool-skin and warm-layer effects on sea surface temperature, *J. Geophys. Res.*, *101*, 1295–1308.

Font, J., G. Lagerloef, D. Le Vine, A. Camps, and O. Z. Zanife (2003), The determination of surface salinity with SMOS—Recent results and main issues, *Proc. Geosci. Remote Sens. Symp. (IGARSS'03)*, *1*, 7–9.

Gaiser, P. W., et al. (2004), The WindSat spaceborne polarimetric microwave radiometer: Sensor description and early orbit performance, *IEEE Trans. Geosci. Remote Sens.*, *42*, 2347–2361.

Gemmrich, J. R., and D. M. Farmer (1999), Observations of the scale and occurrence of breaking surface waves, *J. Phys. Oceanogr.*, *29*, 2595–2606.

Gladstone, J. H., and T. P. Dale (1863), Researches on the refraction, dispersion, and sensitiveness of liquids, *Philos. Trans. R. Soc. London*, *153*, 317–343.

Guo, J., L. Tsang, W. Asher, K.-H. Ding, and C.-T. Chen (2001), Applications of dense media radiative transfer theory for passive microwave remote sensing of foam covered ocean, *IEEE Trans. Geosci. Remote Sens.*, *39*, 1019–1027.

Hallikainen, M. T., F. T. Ulaby, and M. Abdelrazik (1986), Dielectric properties of snow in the 3 to 37 GHz range, *IEEE Trans. Antennas Propag.*, *AP-34*, 1329–1340.

Hashin, Z., and Z. Shtrikman (1962), A variational approach to the theory of the effective magnetic permeability of multiphase materials, *J. Appl. Phys.*, *33*(10), 3125–3131.

Hsu, W. Y., W. G. Holtje, and J. R. Barkley (1988), Percolation phenomena in polymer/carbon composites, *J. Mater. Sci. Lett.*, *7*, 459–462.

Jessup, A. T., C. J. Zappa, M. R. Loewen, and V. Hesany (1997), Infrared remote sensing of breaking waves, *Nature*, *385*, 52–55.

Kärkkäinen, K. K., A. H. Sihvola, and K. I. Nikoskinen (2000), Effective permittivity of mixtures: Numerical validation by the FDTD method, *IEEE Trans. Geosci. Remote Sens.*, *38*, 1303–1308.

Kirkpatrick, S. (1973), Percolation and conduction, *Rev. Mod. Phys.*, *45*(4), 574–588.

Klein, L. A., and C. T. Swift (1977), An improved model for the dielectric constant of sea water at microwave frequencies, *IEEE Trans. Antennas Propag.*, *AP-25*, 104–111.

Koga, M. (1982), Bubble entrainment in breaking wind waves, *Tellus*, *34*, 481–489.

Koh, G. (1992), Effective dielectric constant of a medium with spherical inclusions, *IEEE Trans. Geosci. Remote Sens.*, *30*, 184–186.

Kolovayev, P. A. (1976), Investigation and statistical size distribution of wind produced bubbles in the near-surface ocean layer, *Oceanology*, *15*, 659–661.

Lamarre, E., and W. K. Melville (1991), Air entrainment and dissipation in breaking waves, *Nature*, *351*, 469–472.

Landauer, R. (1978), Electrical conductivity in inhomogeneous media, *AIP Conf. Proc.*, *40*(1), 2–45.

Leifer, I., and G. de Leeuw (2006), Bubbles generated from wind-steepened breaking waves: 1. Bubble plume bubbles, *J. Geophys. Res.*, *111*, C06020, doi:10.1029/2004JC002673.

Leifer, I., G. Caulliez, and G. de Leeuw (2006), Bubbles generated from wind-steepened breaking waves: 2. Bubble plumes, bubbles, and wave characteristics, *J. Geophys. Res.*, *111*, C06021, doi:10.1029/2004JC002676.

Lewis, E. R., and S. E. Schwartz (2004), *Sea Salt Aerosol Production: Mechanisms, Methods, Measurements, and Models*, *Geophys. Monogr. Ser.*, vol. 152, American Geophysical Union, Washington.

Looyenga, H. (1965), Dielectric constants of heterogeneous mixtures, *Physica*, *31*, 401–406.

Mallet, P., C. A. Guérin, and A. Santenac (2005), Maxwell-Garnett mixing rule in the presence of multiple scattering: Derivation and accuracy, *Phys. Rev. B*, *72*, 014205.1–014205.9.

Meissner, T., and F. J. Wentz (2004), The complex dielectric constant of pure and sea water from microwave satellite observations, *IEEE Trans. Geosci. Remote Sens.*, *42*, 1836–1849.

Melville, W., E. Terrill, and L. Ding (1995), Field measurements of air entrainment by breaking waves, in *Air-Water Gas Transfer*, edited by B. Jähne and E. Monahan, pp. 285–295, Verlag & Studio, Hanau, Germany.

Militskii, Y. A., V. Y. Raizer, E. A. Sharkov, and V. S. Etkin (1977), Scattering of microwave radiation by foamy structures, *Radio Eng. Electron Phys.*, *22*(11), 46–50.

Militskii, Y. A., V. Y. Raizer, E. A. Sharkov, and V. S. Etkin (1978), Thermal radio emission from foam structures, *Sov. Phys. Tech. Phys.*, *23*, 601–602.

Monahan, E., and D. Woolf (1989), Comments on "Variations of whitecap coverage with wind stress and water temperature", *J. Phys. Oceanogr.*, *19*, 706–709.

Odelevskiy, V. I. (1951), Calculation of generalized conductance of heterogeneous systems. 1: Matrix two phase systems with nonelongated inclusions, *Zh. Tekh. Fiz.*, *21*, 667–685.

Peltzer, R. D., and O. M. Griffin (1988), Stability of a three-dimensional foam layer in seawater, *J. Geophys. Res.*, *93*, 10,804–10,812.

Pinet, P. (1992), *Oceanography*, 571 pp., West, St. Paul, Minn.
Polder, D., and J. H. Van Santen (1946), The effective permeability of mixtures of solids, *Physica*, *XII*(5), 257–271.
Raizer, V. (2007), Macroscopic foam-spray models for ocean microwave radiometry, *IEEE Trans. Geosci. Remote Sens.*, *45*(10), 3138–3144.
Raizer, V. Ya., and E. A. Sharkov (1981), Electrodynamic description of densely packed dispersed systems, *Izv. Radiophys. Quantum Electron.*, *24*, 553–560.
Reising, S. C., W. E. Asher, and L. A. Rose (2002), Polarimetric emissivity of whitecaps experiment (POEWEX): Preliminary Results, WindSat Science Workshop, November, Noesis, Inc., Arlington, VA.
Reul, N., and B. Chapron (2003), A model of sea-foam thickness distribution for passive microwave remote sensing applications, *J. Geophys. Res.*, *108*(C10), 3321, doi:10.1029/2003JC001887.
Rose, L. A., W. E. Asher, S. C. Reising, P. W. Gaiser, K. M. St Germain, D. J. Dowgiallo, K. A. Horgan, G. Farquharson, and E. J. Knapp (2002), Radiometric measurements of the microwave emissivity of foam, *IEEE Trans. Geosci. Remote Sens.*, *40*, 2619–2625.
Rosenkranz, P., and D. Staelin (1972), Microwave emissivity of ocean foam and its effect on nadiral radiometric measurements, *J. Geophys. Res.*, *77*, 6528–6538.
Sihvola, A. (1999), *Electromagnetic Mixing Formulas and Applications*, 284 pp., The Institute of Electrical Engineers, London.
Sihvola, A., S. Saastamoinen, and K. Heiska (1994), Mixing rules and percolation, *Remote Sens. Rev.*, *9*(1–2), 39–50.
Sihvola, A. H., and J. A. Kong (1988), Effective permittivity of dielectric mixtures, *IEEE Trans. Geosci. Remote Sens.*, *26*, 420–429.
Stogryn, A. P. (1997), Equations for the permittivity of sea water, *Report to NRL Washington DC*, 11 pp., GenCorp Aerojet, Azusa, CA.
Thorpe, S. (1982), On the clouds of bubbles formed by breaking wind-waves in deep water, and their role in air-sea gas transfer, *Philos. Trans. R. Soc. London*, *A304*, 155–210.
Thorpe, S. (1984), The effect of Langmuir circulation on the distribution of submerged bubbles caused by breaking wind waves, *J. Fluid Mech.*, *142*, 151–170.
Troitsky, V. (1962), Radio emission of the moon, its physical state, and the nature of its surface, in *The Moon*, edited by Z. Kopal and Z. Mikhailov, pp. 475–489, Elsevier, New York.
Tsang, L., J. A. Kong, and R. T. Shin (1985), *Theory of Microwave Remote Sensing*, *Wiley Ser. In Remote Sensing*, 613 pp., Wiley & Sons, New York.
Ulaby, F., R. Moore, and A. Fung (1986), *Microwave Remote Sensing: Active and Passive, From Theory to Applications*, vol. III, 2162 pp., Artech House, Dedham, Massachusetts.
van Beek, L. K. H. (1967), Dielectric behaviour of heterogeneous systems, in *Progress in Dielectrics*, 7, edited by J. B. Birks, pp. 69–114, Iliffe Books, Ltd., London.
Walsh, A., and P. Mulhearn (1987), Photographic measurements of bubble population from breaking waves at sea, *J. Geophys. Res.*, *92*, 14,553–14,565.
Wentz, F. (1974), The effect of surface roughness on microwave sea brightness temperatures, *Contractor Rep. 3-35345*, NOAA, Silver Spring, Md.
Wilheit, T. T. (1978), A review of applications of microwave radiometry to oceanography, *Boundary Layer Meteorol.*, *13*, 277–293.
Williams, G. F. (1971), Microwave emissivity measurements of bubbles and foam, *IEEE Trans. Geosci. Electron*, *GE-9*, 221–224.
Wu, F., and K. W. Whites (2001), Quasi-static effective permittivity of periodic composites containing complex shaped dielectric particles, *IEEE Trans. Antennas Propag.*, *49*, 1174–1182.
Wu, J. (1994), Bubbles in the near-shore ocean: Their various structures, *J. Phys. Oceanogr.*, *24*, 1956–1965.
Zhang, Y., Y. E. Yang, and J. A. Kong (2003), A composite model for estimation of polarimetric thermal emission from foam-covered wind-driven ocean surface, *Prog. Electron. Res.*, *PIER 41*, 143–190.

M. D. Anguelova, Remote Sensing Division, Naval Research Laboratory, Code 7223, 4555 Overlook Avenue Southwest, Washington, DC 20375-5320, USA. (maggie.anguelova@nrl.navy.mil)